

Studies on Relationship between a Microtubule-associated Protein Tau and Alzheimer's
Disease Progression and Drug Discovery Targeting Tau

A Dissertation Submitted to
the Graduate School of Life and Environmental Sciences,
the University of Tsukuba
in Partial Fulfillment of the Requirements
for the Degree of Doctor of Philosophy in Biological Science
(Doctoral Program in Biological Sciences)

Tomohiro ONISHI

Table of Contents

Abstract	1
Abbreviations	4
General Introduction	6
Part 1	10
Abstract	11
Introduction	12
Materials and Methods	14
Results	21
Discussion	25
Figures	29
Part 2	61
Abstract	62
Introduction	63
Materials and Methods	65
Results	71
Discussion	75
Figures	79
General Discussion	100
Acknowledgements	104
References	106

Abstract

Alzheimer's disease (AD) is a neurodegenerative disorder leading to a progressive loss of cognitive function and is pathologically characterized by senile plaques and neurofibrillary tangles (NFTs). Microtubule-associated protein tau (MAPT) is a major constituent of NFTs, and its hyperphosphorylation is considered one of causes of AD. Mutations in the MAPT gene are known to cause familial neurodegenerative diseases such as frontotemporal dementia with parkinsonism linked to chromosome 17 (FTDP-17). The purpose of this study was to understand the mechanism of tau neurotoxicity and to discover a tau-targeting drug. I generated a novel mouse model of tauopathy harboring mutant tau and clarified etiology of tau in neurodegenerative diseases. And, I discovered a drug inhibiting tau phosphorylation and assessed its therapeutic efficacy in AD mouse model.

In the first chapter, I describe a transgenic mouse, named TPR50, harboring human tau with an FTDP-17 mutation P301S. TPR50 mice exhibited age-related increase in tau phosphorylation in the hippocampus. Insolubilization and intracellular accumulation of tau were observed in the hippocampus by 9 months of age. While, behavioral function related to cognition and memory was already impaired at earlier age. At that age, decrease in axonal transport in the septo-hippocampal pathway was observed, and expression of microtubule (MT)-related proteins and MT hyperdynamics in the hippocampus were abnormally increased. They might account for behavioral dysfunction, suggesting that impaired axonal function rather than accumulation of insoluble tau may be linked with neural dysfunction in TPR50 mice. TPR50 mouse is a valuable model to study progression of tauopathies.

In the second chapter, I describe a novel glycogen synthase kinase-3 (GSK-3) inhibitor that suppresses tau phosphorylation. By high-throughput screening and chemical

modification, I found 2-methyl-5-(3-{4-[(S)-methylsulfinyl]phenyl}-1-benzofuran-5-yl)-1,3,4-oxadiazole (MMBO), which displays high selectivity for GSK-3 and brain penetration following oral administration. When administered to a transgenic mouse model of AD, MMBO significantly decreased phosphorylated tau in the hippocampus. Chronic administration of MMBO suppressed tau pathology as assessed by immunoreactivity of AT8, which is a phosphorylated tau antibody. In addition, MMBO significantly improved memory and cognitive deficits in the AD mouse model. These results indicate that pharmacological GSK-3 inhibition ameliorates behavioral dysfunction with suppression of tau phosphorylation in an AD mouse model.

Taken together, I conclude that improvement of axonal dysfunction due to abnormal tau is a novel therapeutic concept in neurodegenerative diseases such as AD, and inhibition of tau phosphorylation is a promising approach based on the concept.

Abbreviations

A β	amyloid β
AD	Alzheimer's disease
FTDP-17	frontotemporal dementia with parkinsonism linked to chromosome 17
FTLD	frontotemporal lobar degeneration
GSK-3	glycogen synthase kinase-3
MT	microtubule
NFTs	neurofibrillary tangles
PHFs	paired helical filaments
SEM	standard error of the mean
Tg	transgenic
WT	wild type

General Introduction

Alzheimer's disease (AD) is the most common cause of dementia, accounting for 60-80% of dementia cases (alz.org: alzheimer's association a). In Japan more 4.6 million people are living with dementia. And this number is expected to rise significantly because Japan is facing unprecedented aging society (alz.org: alzheimer's association b). Worldwide, over 46 million people are estimated to be living with dementia, and the number of people with dementia is predicted to reach 74.7 million by 2030 and 131.5 million by 2050, if effective disease modifying therapies are not developed (Alzheimer's Disease International: World Alzheimer Report 2015). Current available therapies for AD only provide symptomatic relief and cannot suppress or halt disease progression. A disease modifying therapy, which is based on pathomechanism of AD, becomes a central focus of drug discovery. Therefore, there is a pressing need to understand pathogenesis more deeply for developing disease modifying therapies.

The two core pathological hallmarks of AD are senile plaques and neurofibrillary tangles (NFTs). And, targeting these pathologies has been developed as therapeutic approaches. In the original hypothesis, senile plaques consisting of amyloid β ($A\beta$) was thought to trigger neuronal dysfunction. The fact that mutations in APP, PSEN1, and PSEN2 genes, which code proteins involved in $A\beta$ production, cause familial types of AD would support the hypothesis. However, several drug candidates targeting $A\beta$ have failed in clinical trials recently, and many researchers now believe that those intervention was too late, and treatments that target $A\beta$ should be tested in earlier stage of the disease rather than in late-stage disease (Golde et al., 2011). In contrast, recent study using large number of postmortem brains clearly showed NFT formation is strongly linked with disease progression such as disease onset and cognitive decline in AD as a driver (Murray et al., 2015). Therefore, interest in NFT and its constituent

microtubule (MT)-associated protein tau as a drug target is increasing. In diseased brain, tau is abnormally hyperphosphorylated at specific sites (Grundke-Iqbal et al., 1986; Friedhoff et al., 2000), and hyperphosphorylation of tau is thought to result in its pathological aggregation forming NFTs. Ultrastructural studies on AD brain specimens revealed that NFTs are primarily made of paired helical filaments (PHFs), that is, fibrils of 10 nm in diameter that form pairs with a helical tridimensional conformation at a regular periodicity of 65 nm (Kidd, 1963, 1964; Wisniewski et al., 1976). This aggregate can stress out neurons. While, tau functions as a modifier of MT stability under physiological condition (Drechsel et al., 1992; Lee et al., 1998; Dixit et al., 2008). Hyperphosphorylation of tau reduces the binding to MT. Consequently, the increased pool of soluble tau may trigger the disintegration of MTs (Grundke-Iqbal et al., 1986; Goedert et al., 1995). Actually, invariably accompanying NFTs are the neuropil threads, which are thought to result from the breakdown of dendrites and axons of the tangle-bearing neurons, suggesting that dysregulation of tau might cause MT abnormality. Moreover, interestingly, mutations in the coding and intronic regions of MAPT, the gene encoding tau, are known to cause familial forms of neurodegenerative disease named FTDP-17 which is adjacent to AD (Hutton et al., 1998; Poorkaj et al., 1998; Spillantini et al., 1998). Taken together, understanding mechanism underlying pathogenesis of tau is valuable for discovering a novel therapeutic strategy in neurodegenerative disease including AD.

Here I summarize my findings on detailed mechanism of tau toxicity and therapeutic strategy of tau-targeting drug by using animal models. In part 1, I generated novel Tg mice (TPR50) expressing human tau with a P301S mutation and assessed the biochemical and behavioral phenotypes. The P301S mutation is one of the major

mutations in FTDP-17, and is linked with early onset of disease progression and strong functional influences (Bugiani et al., 1999; Goedert et al., 1999; Yasuda et al., 2000; Lossos et al., 2003; Werber et al., 2003). In second part, I report therapeutic potential of the drug targeting tau in AD mouse model. As described above, hyperphosphorylation of tau is thought to result in its pathological aggregation and phosphorylation is contributed by some kinases. GSK-3 is reported to phosphorylate tau affecting microtubule rearrangement in vitro (Lovestone et al., 1996; Wagner et al., 1996) and also to be associated with NFTs in AD (Pei et al., 1997 and 1999), suggesting that inhibition of GSK-3 is a good therapeutic target. In this study, I discovered a novel selective GSK-3 inhibitor, and validated its potential in an AD mouse model.

Part I

Early-Onset Cognitive Deficits and Axonal Transport Dysfunction in P301S Mutant Tau

Transgenic Mice

Abstract

AD and FTLN are neurodegenerative “tauopathies” characterized by hyperphosphorylated tau accumulation and NFTs. The P301S mutation of tau, a causal mutation of a familial type of FTLN, is believed to be involved in neurodegenerative progression. I developed a transgenic mouse, named TPR50, harboring human P301S tau. Tau phosphorylation in the hippocampus of TPR50 mice increased with age, particularly at S202/T205. Insolubilization and intracellular accumulation of tau were detected in the hippocampus by 9 months of age. Expression of calbindin was significantly reduced in 6- and 9-month-old TPR50 mice but not in 3-month-old mice. TPR50 mice demonstrated cognitive dysfunction at 5 months. At this age or earlier, although no intracellular tau accumulation was observed in the hippocampus, abnormally increased MT-related proteins and MT hyperdynamics in the hippocampus, and impaired axonal transport in the septo-hippocampal pathway were already observed. Therefore, cognitive dysfunction in TPR50 mice may result from early MT dysfunction and impaired axonal transport rather than accumulation of insoluble tau and neurodegeneration. TPR50 mice are a valuable new model to study progression of tauopathies at both the behavioral and neurocellular levels and may also prove useful for testing new therapies for neurodegenerative diseases.

Introduction

NFT, consisting of the MT-associated protein tau are a pathological hallmark of AD and FTLD such as Pick disease, progressive supranuclear palsy, and corticobasal degeneration (Goedert et al., 1988; Lee et al., 2001). The strong temporal correlation between NFT formation, neurodegeneration, and symptom progression indicates that tau is a key molecule in disease pathogenesis. Indeed, these diseases are collectively termed tauopathies.

Under physiological conditions, tau functions as a modifier of MT stability (Drechsel et al., 1992; Lee et al., 1998; Dixit et al., 2008). Hyperphosphorylation of tau reduces the binding to MT. Consequently, the increased pool of soluble tau may trigger the disintegration of MTs (Grundke-Iqbal et al., 1986; Goedert et al., 1995). Mutations in the coding and intronic regions of MAPT, the gene encoding tau, are known to cause familial forms of FTLD (FTDP-17) (Hutton et al., 1998; Poorkaj et al., 1998; Spillantini et al., 1998). Several mutant tau transgenic (Tg) mouse lines have been generated to model tau pathology and neurodegenerative phenotypes (Götz and Ittner, 2008), some of which exhibit abnormal tau accumulation and impaired axonal function (Lewis et al., 2000; Zhang et al., 2004; Ittner et al., 2008).

In humans, the P301S mutation causes early onset of disease progression and strong functional influences (Bugiani et al., 1999; Goedert et al., 1999; Yasuda et al., 2000; Lossos et al., 2003; Werber et al., 2003). Biochemical studies have shown that the P301S mutation reduces the ability of MT assembly (Bugiani et al., 1999) and enhances heparin-induced tau filament formation (Goedert et al., 1999). Two lines of Tg mice expressing P301S mutant 4R0N and 4R1N tau isoforms have been reported (Allen et al.,

2002; Yoshiyama et al., 2007), and both lines develop NFT-like pathology and neurodegeneration. Memory impairment was also reported in one of these lines (Takeuchi et al., 2011). However, definitive mechanism of toxicity by mutant tau is still unclear. Therefore, I conducted this study in order to understand a pathophysiological role of tau in disease progression. I generated novel Tg mice (TPR50) expressing the longest form (4R2N) of tau with a P301S mutation and assessed the biochemical and behavioral phenotypes to further investigate the mechanisms underlying age-dependent tau accumulation, neurotoxicity, and behavioral sequelae. I also examined tau pathophysiology, neural function, MT-related proteins, and axonal function of TPR50 mice by behavioral and biochemical approaches. These mice exhibited age-dependent abnormal tau accumulation and motor deficits as expected. In addition, they showed early-onset of cognitive impairment and disrupted axonal transport in the septo-hippocampal pathway.

Materials and Methods

Animals

TPR50 mice were generated by microinjection of a vector encoding a P301S mutant of the longest human tau isoform (4R2N) under the control of the mouse prion promoter (Supplementary Figure 1) into single-cell embryos harvested from BDF1 mice and then backcrossed more than 10 times with C57BL/6J mice. Only male mice were used in this study. They were housed in groups and kept on a 12h-light/12h-dark schedule and provided ad libitum access to food and water. All animals were maintained and sacrificed according to the guidelines of the Takeda Experimental Animal Care and Use Committee.

Antibodies

Antibodies against the following proteins were used in this study: AT270, AT8, HT7 (Innogenetics, Ghent, Belgium), pS214-tau, pS262-tau, pS396-tau (Invitrogen, Carlsbad, CA, USA), Ab-3 (Thermo Fisher Scientific, Fremont, CA, USA), synaptophysin, acetylated tubulin, α -tubulin, β -actin (Sigma, St. Louis, MO, USA), synaptotagmin (Enzo, New York, NY, USA), kinesin heavy chain, PSD-95, and calbindin (Millipore, Bedford, MA, USA).

SDS-PAGE and Western blotting

Hippocampi isolated from Tg and WT mice were homogenized in lysis buffer (50 mM Tris-HCl, 5 mM EDTA, 1 mM EGTA, 100 mM NaCl, 1% NP-40, and 2.5% sodium deoxycholate, pH7.5) supplemented with protease inhibitors [1.37 mg/L pepstatin A, 25

KIU/mL aprotinin, 1 nM microcystin LR, 1 nM MG115, 40 nM leupeptin and 100 nM 4-(2-aminoethyl)benzenesulfonyl fluoride (ABSF) HCl] and phosphatase inhibitors (30 mM NaF, 5 mM sodium diphosphate, and 2 nM sodium orthovanadate). The homogenate was centrifuged at 10,000 g for 10 minutes and the supernatant taken as the soluble protein fraction. Total protein concentration was determined using the BCA assay kit (Pierce, Rockford, IL, USA). Equal amounts of protein (1-20 µg depending on the protein of interest) were separated by SDS-PAGE on 10% polyacrylamide gels, then electrophoretically transferred to 0.45 µm poly-vinylidene difluoride membranes (Millipore) and blocked for 1 h in BlockAce (DS Pharma Biomedical, Osaka, Japan). After blocking, the membranes were probed with primary antibodies followed by labeling with horseradish peroxidase (HRP)-coupled secondary antibodies (Amersham, Piscataway, NJ, USA). Immunolabeling was visualized by a chemiluminescence reagent (Immunostar; Wako, Osaka, Japan) using a LAS1000 imaging system (Fujifilm, Tokyo, Japan) or ImageQuant LAS4000 (GE healthcare, Pittsburgh, PA, USA). Quantitative densitometric analyses were performed with Image Gauge (Fujifilm) or ImageQuant TL (GE healthcare). Values presented are derived from densitometry arbitrary units (A.U.). With regard to immunoblot of tau, the bands including all tau species were selected and analyzed.

Preparation of insoluble tau

Insoluble aggregated tau was prepared by the sarkosyl extraction methods, described previously (Sahara et al., 2004; Taniguchi et al., 2005; Uno et al., 2009). In brief, lysis buffer-insoluble pellets were rehomogenized with 0.5 M NaCl containing 10% sucrose and incubated in 1% sarkosyl for 1 h at 37°C. After centrifugation at 256,000 g for 15

minutes, the pellets were resuspended by ultrasonication in phosphate buffered saline to yield the sarkosyl insoluble fraction.

RAB-RIPA-formic acid (FA) extraction

RAB-RIPA-FA extraction was performed by using a previously described method (Ishihara et al., 1999, 2001; Eckermann et al., 2007; Uno et al., 2009). Brain tissue was homogenized in ice-cold high-salt RAB buffer [0.1 M morpholineethanesulfonic acid (MES), 1 mM EGTA, 0.5 mM MgSO₄, 0.75 M NaCl, 0.02 M NaF, 100 μM ABSF, and protease inhibitors (Complete Mini, Roche Applied Science, Mannheim, Germany), pH 7.0], and the sample was centrifuged at 50,000 g for 20 minutes at 4°C. The supernatant was boiled for 5 minutes and then centrifuged at 10,000 g for 20 minutes at 4°C. The resulting supernatant contains the soluble tau fraction (RAB fraction). To remove myelin and associated lipids, RAB insoluble pellets were re-extracted with 1 M sucrose/RAB buffer and centrifuged at 100,000 g for 30 minutes at 4°C. The pellets were suspended in RIPA buffer (50 mM Tris-HCl, 5 mM EDTA, 1 mM EGTA, 30 mM NaF, 5 mM sodium diphosphate, 2 μM pepstatin A, 100 mM NaCl, 1% NP-40, 0.25% sodium deoxycholate, 1 μM microcystin LR, 40 μM leupeptin, 100 μM ABSF, 2 mM sodium orthovanadate, 1 μM MG115, pH 7.6) and centrifuged as mentioned above to obtain the supernatants (RIPA fraction). Finally, the RIPA insoluble pellets were re-extracted with 70% FA.

Immunohistochemistry

Dissected hemibrains were fixed in 4% paraformaldehyde (Wako) for 24 h. Fixed hemibrains were embedded and frozen in freezing medium (OCT Tissue-Tek 4583;

Sakura Finetechnical, Tokyo, Japan) and sliced into 20- μ m-thick sections using a cryostat (CM1850; Leica, Nussloch, Germany). These sections were mounted onto silane-coated slides (Matsunami, Osaka, Japan). After blocking with BlockAce containing 3% fetal bovine serum, the slides were probed with a primary antibody against total tau (HT7, 1:2000 dilution), followed by an HRP-coupled secondary antibody (Dako, Glostrup, Denmark). Immunolabeling was detected by 3,3'-diaminobenzidine tetrahydrochloride staining (Dako). Images were captured using Nanozoomer and NDP scan software (Hamamatsu Photonics, Hamamatsu, Japan).

Bielschowsky silver staining

Bielschowsky silver staining was performed as described previously (Bellucci et al., 2006), with minor modifications. The dissected brain was fixed in 4% paraformaldehyde (Wako) for 24 h. The right hemisphere was cut in the coronal plane and the left hemisphere was cut in the sagittal plane. Samples were embedded in paraffin and cut into 4- μ m-thick sections. After deparaffinization, the sections were stained with 20% silver nitrate solution for 20 minutes, rinsed in distilled water, and stained with ammonium silver solution for 20 minutes. After washing with 0.1% ammonium hydroxide solution, the sections were put in ammonium silver solution containing formaldehyde, monohydrate citric acid, and concentrated nitric acid for optimal staining. The sections were then rinsed three times in distilled water, placed in 5% sodium thiosulfate solution for 5 minutes, dehydrated through increasing concentrations of ethanol and xylene, and assembled.

Behavioral assessments

Y-maze: The Y-maze has three arms, 42 cm in length and 3 cm in width, projecting at equal angles and all colored black (BrainScience Idea, Osaka, Japan). The walls of the maze are 12-cm tall, and angled at 16.25° from the vertical. Mice were initially placed within one arm, and the sequence and number of arm entries were recorded for each mouse over a period of 8 minutes. An arm choice was defined as both forepaws and hindpaws fully entering the arm. The device was cleaned with 10% ethanol between trials. The percentage of triads in which all three arms were entered (ABC, CAB, or BCA but not BAB) was recorded as a spontaneous alternation to estimate short-term memory. In addition, the number of total arm entries served as an indicator of general locomotor activity.

Novel object recognition: The box and objects used were purchased from BrainScience Idea (Osaka, Japan). The box was 30 × 30 × 30 cm and colored neutral gray. The two acquisition trial objects (object A and A*) were white ceramic cylinders and the novel object (B) was a black wooden rectangular parallelepiped. In the acquisition test, the identical objects (objects A and A*) were symmetrically placed in the box. Each animal was placed in the corner of the box with head turned toward the wall and allowed 5 minutes of exploration. The devices were cleaned with 10% ethanol between trials. The retention test was administered 24 h later. After replacing one of the objects with a novel object (object B), mice were reintroduced into the box for a 5-minute retention test. The time spent exploring the objects and the number of approaches was measured during both tests. Retention was represented by how long the animals explored the novel object versus the familiar object (exploratory preference).

Rotarod: The apparatus consisted of a bar, which was 3.0 cm in diameter and 40 cm in length and was subdivided into five areas by disks (Muromachi Kikai, Tokyo, Japan).

The mice were given a 300-s training session on the rotating rod at 4 rpm 1 day before the three test trials. Each mouse was placed on the rotating rod with its head pointed in the direction opposite that of rotation so that the mouse progressed forward to maintain balance. Each trial for each mouse was separated by 1 h. The apparatus was cleaned with 10% ethanol between trials. During the testing phase, the mice were subjected to three consecutive trials at 10 rpm over 180 s and the mean latency to fall was recorded.

MT dynamics assay

The methods used for in vivo measurements of MT dynamics included ^2H isotope labeling and application of the KineMed proprietary biomarker platform, as previously described (Fanara et al., 2007; Fanara et al., 2010; Barten et al., 2012; Fanara et al., 2012).

Evaluation of axonal transport

Retrograde axonal transport was monitored by injection of 0.5 μL of 5% Fluoro-Gold (Fluorochrome, Denver, CO) into the hippocampus. The injection site was AP -2.3 mm, ML -2.0 mm, and DV -2.0 mm relative to bregma. Three days after the injection, the mice were anesthetized and transcardially perfused with phosphate-buffered saline (pH 7.4), and then 4% paraformaldehyde. Fixed brains were embedded and frozen in freezing medium and sliced into 20- μm -thick sections using a cryostat. The sections including the medial septum (1.10 mm relative to bregma) were selected and mounted onto silane-coated slides with mounting medium (VECTASHIELD; VECTOR, Burlingame, CA) and coverslipped. Images were captured using an ECLIPS E800M microscope (Nikon, Tokyo, Japan) and a camera (DXM1200, Nikon). Fluorescent cells in

the medial septum were counted with Image-Pro Plus software (Media Cybernetics, Rockville, MD, USA).

Statistical analysis

Data are expressed as mean \pm SEM and were analyzed by Student's *t*-tests or Welch's test for comparisons between WT and Tg mice. $p \leq 0.05$ was considered statistically significant. Student's *t*-tests were also used for comparisons in the novel object recognition test. Analyses were performed using SAS system 8 software (SAS Institute, Cary, NC, USA).

Results

Human tau expression and phosphorylation in TPR50 mice

To examine tau-induced toxicity in vivo, I generated Tg mice expressing human P301S tau under the control of the mouse prion promoter. I established 7 lines of Tg mice (TPR16, 50, 56, 72, 82, 96, and 100, Supplementary Figure 1). The line with the highest P301S tau expression (TPR50) was backcrossed more than 10 times with C57BL/6J mice, and used in this study because it was expected to display the most severe phenotypes. These TPR50 mice expressed human mutant tau throughout the brain (Figure 1A). Motor deficits were observed at 8.5 months of age but not at 5 months (Figure 1B). When lifted by the tail, these mice crossed their hind limbs, a behavior endophenotype of tauopathy-associated motor dysfunction. In addition to motor deficits, TPR50 mice had a lower mean body weight than age-matched WT mice, and this difference increased with age (Figure 1C). Moreover, life expectancy was reduced in Tg mice (Supplementary Figure 2). To evaluate the phosphorylation state of human tau, total proteins were isolated from the hippocampi of 9.5-month-old TPR50 and WT mice and analyzed by Western blotting and densitometry (Figure 2A). Quantitative analysis revealed significant increase in total human tau expression in the hippocampus of TPR50 mice (Figure 2G). In addition, human tau in Tg mice was phosphorylated at T181, S202/T205, S214, S262, and S396, sites that are often phosphorylated in human disease (Figures 2A–F). To examine whether phosphorylation status is age-dependent, pS202/pT205-, pS262-, and pS396-tau expression levels were examined in 3-, 6-, and 9-month-old TPR50 and WT mice. Although total tau expression was similar at every age (Figure 3E), pS202/pT205-tau increased progressively with age in TPR50 mice

(Figure 3B). In addition, tau phosphorylated at S262 and S396 also increased slightly with age in Tg mice, although the extent of increase was less than that of pS202/pT205-tau (Figures 3C and 3D).

Age-dependent intracellular accumulation and insolubilization of tau in TPR50 mice

Accumulation of filamentous tau in NFTs is a characteristic feature of neurodegenerative tauopathies, and some studies reported that tau transgenic mouse models do exhibit age-dependent NFT-like inclusions (Götz and Ittner, 2008). We measured age-dependent tau accumulation in the sarkosyl-insoluble protein fractions from the hippocampus of TPR50 mice. Sarkosyl-insoluble tau was first detected in 3-month-old mice, although this was only slightly detected with no significant difference between WT and Tg mice and increased progressively with age (Figures 4A and E). Tau proteins phosphorylated at S202/T205, S262, and S396 were also detected in the sarkosyl-insoluble fraction (Figures 4A–D). The results of RAB-RIPA-FA extraction also revealed a progressively age-dependent increase in insoluble pS202/pT205-tau in TPR50 mice (Supplementary Figure 3). These phenotypes suggest age-dependent, tauopathy-like tau accumulation in TPR50 mice. Intracellular tau accumulation was examined by immunohistochemical analysis (Figure 5). Tau accumulation was observed in hippocampal sections from 9-month-old TPR50 mice (Figures 5C and F) but not in sections from 6-month-old TPR50 mice (Figures 5B and E), although 6-month-old mice expressed comparable levels of soluble tau (Figure 3E).

Cognitive impairments in TPR50 mice

I examined cognitive function in 5-month-old TPR50 mice, an age at which no

significant motor deficits were observed (Figure 1B). In the Y-maze test of short-term spatial memory, spontaneous alternation behavior was significantly impaired in TPR50 mice (Figure 6A). Total arm entries were comparable between WT and Tg mice, indicating no severe motor deficits at this age. The motor phenotype comparable to WT was also confirmed by the rotarod test (Supplementary Figure 4). In the novel object recognition test (Figure 6B), both WT and Tg mice demonstrated comparable exploratory activity around both trial objects (objects A and A*), although Tg mice tended to explore objects for longer period than WT mice. After a 24-hour delay, object A* was replaced with a novel object (B) and the relative time exploring the new vs. familiar object (A) was used as a measure of object recognition. TPR50 mice showed less exploratory preference for the novel object than for the previously presented object compared with WT mice. These results indicate that TPR50 mice have impairments in cognitive function as early as 5 months of age.

Alteration of MT-related proteins and neuronal markers in TPR50 mice

To biochemically examine neural function of TPR50 mice, several proteins involved in MT stabilization or synaptic function were evaluated by Western blotting (Figure 7). Expression of MT-related proteins such as α -tubulin, its acetylated form, and kinesin heavy chain (KHC) were significantly higher in the hippocampus of TPR50 mice (Figures 7B–D). These increases were similarly observed in 3-, 6-, and 9-month-old Tg mice. Simultaneously, neuronal markers such as calbindin, synaptophysin, synaptotagmin, and PSD-95 were also examined. Expression of calbindin was comparable between 3-month-old WT and Tg mice but significantly reduced in 6- and 9-month-old TPR50 mice (Figure 7E). With regard to the expression of synaptophysin,

synaptotagmin, and PSD-95 at up to 9 months of age, there was no significant difference between WT and Tg mice (Figures 7F-H).

MT hyperdynamics and impaired axonal transport in TPR50 mice

Western blotting demonstrated abnormal expression levels of several MT-related proteins in TPR50 mice, suggesting possible changes in MT polymerization and depolymerization (MT dynamics). MT dynamics in 4- and 7-month-old TPR50 and WT mice were assessed in vivo by measuring ^2H label incorporation into newly synthesized MTs. Although no changes in MAP2-associated MT dynamics were observed in 4-month-old TPR50 mice, the dynamics of tau-associated MTs were accelerated in both the cortex and hippocampus (but not the cerebellum) (Figures 8A-C). Similarly, the dynamics of tau-associated MTs were also accelerated in 7-month-old Tg mice (Figures 8D-F). A significant increase in MT dynamics was observed in the MAP2-associated fraction from the cortex and hippocampus of TPR50 mice at this age, and cold stable (CS)-MTs were significantly increased in the cortical fraction.

To examine whether axonal transport in the septohippocampal pathway was impaired in TPR50 mice, the retrograde tracer Fluoro-Gold was injected in the hippocampus of 5-month-old TPR50 and WT mice, and fluorescent dye accumulation was measured in the medial septum (Supplementary Figure 5). The age of 5 months was selected for evaluation because obvious memory and cognitive abnormality was already observed at this age (Figure 6). Consistent with disrupted axonal transport in this pathway, TPR50 mice exhibited significantly fewer labeled septal cells than WT mice (Figure 9).

Discussion

I report the generation and characterization of TPR50, a novel transgenic mouse expressing a human P301S mutant 4R2N tau, and demonstrate that TPR50 is a robust model of progressive neurocellular and behavioral deficit characteristics of human tauopathies. I examined age-related pathophysiology including tau accumulation and neuronal dysfunction in TPR50 mice to confirm that these mice demonstrate similar age-dependent neurocellular deficits and behavioral endophenotypes as previous tau mutant mice. This information would be useful for understanding pathogenesis of human disease and for translational study in drug discovery.

Expression of P301S human tau in TPR50 mice was controlled by the mouse prion promoter, allowing expression throughout the brain (Figure 1B). Total human mutant tau expression in TPR50 mice was significantly increased compared with endogenous wild type mouse tau (Figures 2 and 3). This overexpressed human tau was phosphorylated at multiple sites (T181, S202/T205, S214, S262, and S396) that are known to be phosphorylated in diseased human brains (Friedhoff et al., 2000) (Figure 2). Tau phosphorylation increased with age at some residues in TPR50 mice, particularly at the AT8-reactive site (Figure 3). Together with increasing tau phosphorylation in TPR50 mice, I observed age-dependent formation of insoluble tau in TPR50 mice over 3–9 months of age (Figure 4). As expected from previous studies on other mutant tau Tg mice (Yoshiyama et al., 2007), insoluble tau was also phosphorylated. It has been proposed that phosphorylated tau dissociates from MTs and that these free tau molecules then form aggregates that ultimately lead to NFTs and neuronal destruction (Götz and Ittner, 2008). Indeed, histological analysis using anti-human tau antibody

revealed that tau accumulation is age-dependent (Figure 5). Intracellular tau accumulation was detected at 9 months of age, while 6-month-old TPR50 mice did not show obvious tau accumulation. Bielschowsky silver staining was also examined and revealed a tangle-like pathology in the hippocampus of 9-month-TPR50 mice (Supplementary Figure 6).

Expression of calbindin was significantly lower in 6- and 9-month-old TPR50 mice than in WT mice, while the expression was comparable between these two types of mice at 3 months of age (Figure 7E). Reduced calbindin expression was reported to be an early sign of neurodegeneration in human AD patients (Iritani et al., 2001; Riascos et al., 2011), underscoring the value of TPR50 mice for modeling the early progression of neurodegenerative disease. In contrast, expression of other neuronal markers, including synaptophysin, synaptotagmin, and PSD-95, did not decrease even at 9 months of age (Figures 7F–7H). This observation indicates that TPR50 mice do not have substantial neurodegeneration in the hippocampus by 9 months of age and may also support the idea that decrease in calbindin is an early sign of neurodegeneration.

Motor deficits are observed in most tau Tg mouse models, although the age of onset varies (Lewis et al., 2000; Yoshiyama et al., 2007; Ittner et al., 2008). In this mouse model, deficits were observed at 8.5 months of age (Figure 1). Some transgenic tauopathy models also demonstrated memory dysfunction prior to detectable neuron loss or NFT formation (SantaCruz et al., 2005; Ittner et al., 2008; Takeuchi et al., 2011; Flunkert et al., 2012). Similarly, TPR50 mice showed early-onset memory deficits as revealed by the Y-maze and novel object recognition tests at 5 months of age (Figure 6), when intracellular tau accumulation is not evident yet. At this age, although an increase in sarkosyl-insoluble tau and reduction in calbindin were speculated (Figures 4

and 7), I found MT-related protein expression and MT dynamics were already altered even at an earlier age (3 or 4 months of age) (Figures 7 and 8). Acetylated tubulin is a known marker of MT stability (Black et al., 1989), and the increase in acetylated tubulin and total tubulin may reflect an alteration in MT turnover in TPR50 mice. Although the mechanism for the increase in KHC expression is unknown, it may reflect a compensatory mechanism in response to axonal dysfunction because KHC is linked to axonal transport (Hurd and Saxton, 1996; Stokin et al., 2005; Henthorn et al., 2011). Alternatively, KHC may be upregulated in the presence of greater numbers of kinesin epitopes associated with MT hyperdynamics. Indeed, abnormality of MT dynamics in TPR50 mice was observed in this study with ²H labeling (Figure 8). Age-dependent MT hyperdynamism was also reported in another tau transgenic mouse and in an ALS mouse model (Fanara et al., 2007; Barten et al., 2012), suggesting that MT hyperdynamism may be a common feature of cytoskeletal dysfunction in neurodegenerative disease models. In addition, TPR50 mice impaired retrograde axonal transport in the septohippocampal pathway at 5 months of age (Figure 9). Belarbi and colleagues recently reported that THY-tau22 mice, a tau Tg mouse with G272V and P301S mutations, exhibited impaired retrograde axonal transport in the septohippocampal pathway coincident with tau pathology and loss of ChAT-positive cholinergic neurons in the medial septum (Belarbi et al., 2009, 2011). In contrast, TPR50 mice showed impaired axonal transport prior to intracellular tau accumulation and before neurodegeneration as assessed by the expressions of neuronal/synaptic markers in the hippocampus. Neither intracellular tau accumulation nor drastic neurodegeneration was observed in the septal area at this age (Supplementary Figure 7). Thus, axonal dysfunction in the hippocampus precedes tau pathology and neuronal

death in TPR50 mice but correlates with the onset of cognitive dysfunction.

The triggers for axonal dysfunction in TPR50 mice remain unclear. As shown in Figure 4A, slight amounts of sarkosyl-insoluble tau were already observed even at 3 months of age and they may significantly affect neuronal function. On the other hand, it has been recently emphasized that soluble tau plays an important role in neuronal dysfunction (Wittmann et al., 2001; SantaCruz et al., 2005), and my previous study found that a decrease in soluble phosphorylated tau rescued cognitive impairments in an AD mouse model (Onishi et al., 2011). These observations support the idea that an increase in soluble and phosphorylated tau may perturb neuronal function in TPR50 mice. Taken together, my results strongly suggest that overexpression of soluble tau accelerates MT turnover, and this MT hyperdynamicity results in axonal dysfunction and cognitive impairments in TPR50 mice. This idea is also supported by reports showing therapeutic effects of MT-stabilizing compounds such as paclitaxel and epothilone D on axonal dysfunction and behavioral anomalies in tau Tg mice (Zhang et al., 2005; Brunden et al., 2010; Zhang et al., 2012), suggesting that regulation of tau phosphorylation and stabilization or protection of axon could be a good therapeutic approach.

In this study, I described TPR50 mice, a novel P301S tau Tg mouse model of tauopathy. These mice demonstrate not only age-dependent abnormalities in tau phosphorylation, insoluble tau accumulation, altered expression of neuronal proteins, and age-dependent motor dysfunction described in previous tauopathy models but also early-onset MT hyperdynamicity and cognitive impairments. In addition to studies of FTLD progression and pathogenesis, these mice may be useful for identifying and validating anti-tau therapies to treat neurodegenerative diseases.

Figures

Figure 1. Human tau expression, motor deficits, and decreased body weight in male TPR50 mice. Expression of human tau in WT (A, left) and TPR50 (A, right) mice was immunohistochemically examined with a human tau antibody (male, 9 months of age). TPR50 mice showed age-dependent motor deficits; 8.5-month-old TPR50 mice (B, right) but not 5-month-old TPR50 mice (B, left) clasped their hind limbs when lifted by the tail. Comparison of body weight between WT and TPR50 (Tg) mice at 5, 7, and 9.5 months of age (C). The body weight of TPR50 mice was less than that of WT mice. Data are expressed as mean \pm SEM. ** $p \leq 0.01$ by Welch's test or Student's t -test, $n = 6$.

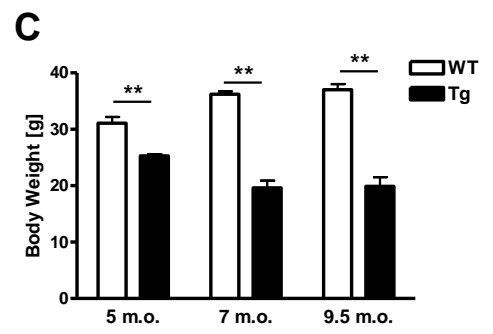
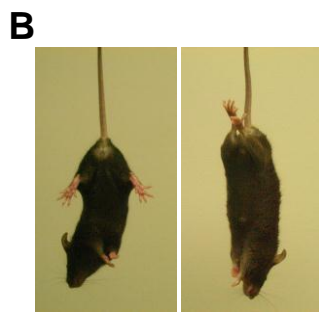


Figure 2. Expression of phosphorylated human tau by TPR50 mice. Western blots probing tau expression in the hippocampal soluble fraction from 9.5-month-old TPR50 mice. Total tau and tau phosphorylated at T181 (detected with AT270), S202/T205 (detected with AT8), S214, S262, and S396 were examined by immunoblot analysis in TPR50 (Tg) and WT mice (A). Comparison of tau expression between TPR50 and WT mice (B–H). Data are expressed as mean \pm SEM. ** $p \leq 0.01$ by Student's *t*-test, $n = 5$ or 6. n.s., not significant.

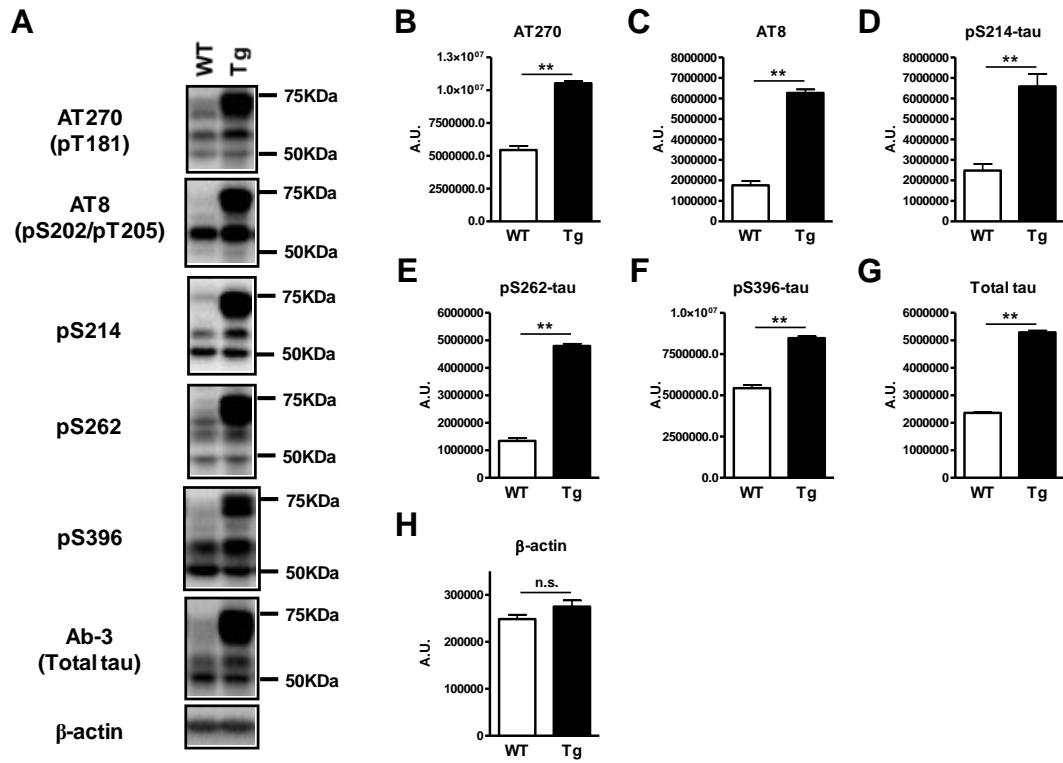


Figure 3. Age-dependent change in tau phosphorylation in TPR50 mice. Tau expression in the soluble fraction from the hippocampus of TPR50 (Tg) and WT mice at 3, 6, and 9 months of age were examined by Western blotting using antibodies against pS202/T205-tau (detected with AT8), pS262-tau, pS396-tau, and total tau (A) and analyzed by densitometry (B–E). Data are expressed as mean \pm SEM. ** $p \leq 0.01$ by Student's *t* test, $n = 5$.

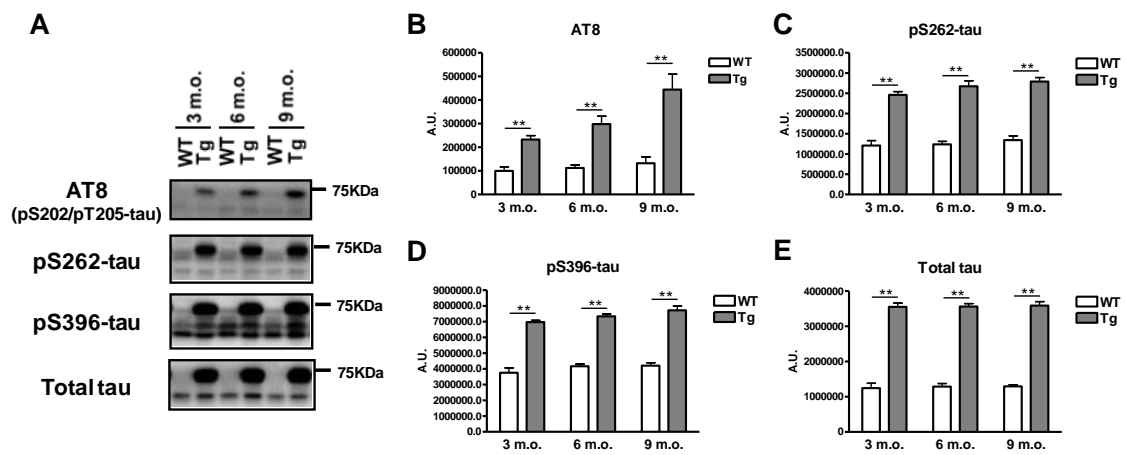


Figure 4. Age-dependent change in sarkosyl-insoluble tau in TPR50 mice. Sarkosyl-insoluble tau levels in the hippocampus of TPR50 (Tg) and WT mice at 3, 6, and 9 months of age were examined by Western blotting using antibodies against pS202/T205-tau (detected with AT8), pS262-tau, pS396-tau, and total tau (A) and analyzed by densitometry (B–E). Data are expressed as mean \pm SEM. ** $p \leq 0.01$ by Student's t test, $n = 5$. n.s., not significant.

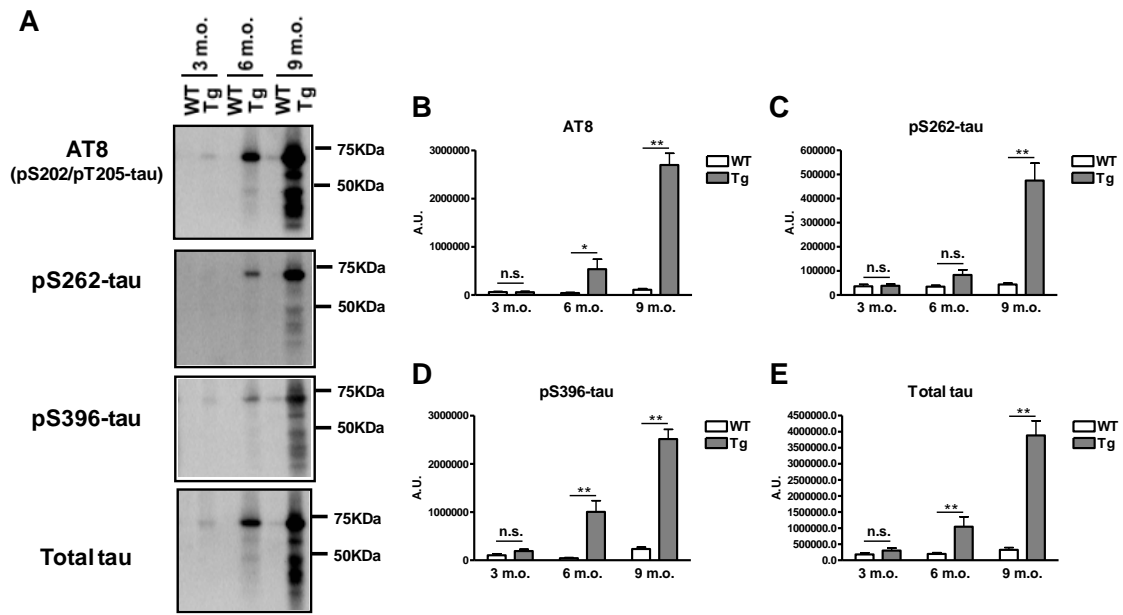


Figure 5. Intracellular tau accumulation in TPR50 mice. Hippocampal sections were examined by immunohistochemistry using human tau antibody (HT7). A, D: 9-month-old WT mice, B, E: 6-month-old TPR50 mice, C, F: 9-month-old TPR50 mice. Bar = 1 mm (A–C); 100 μ m (D–F).

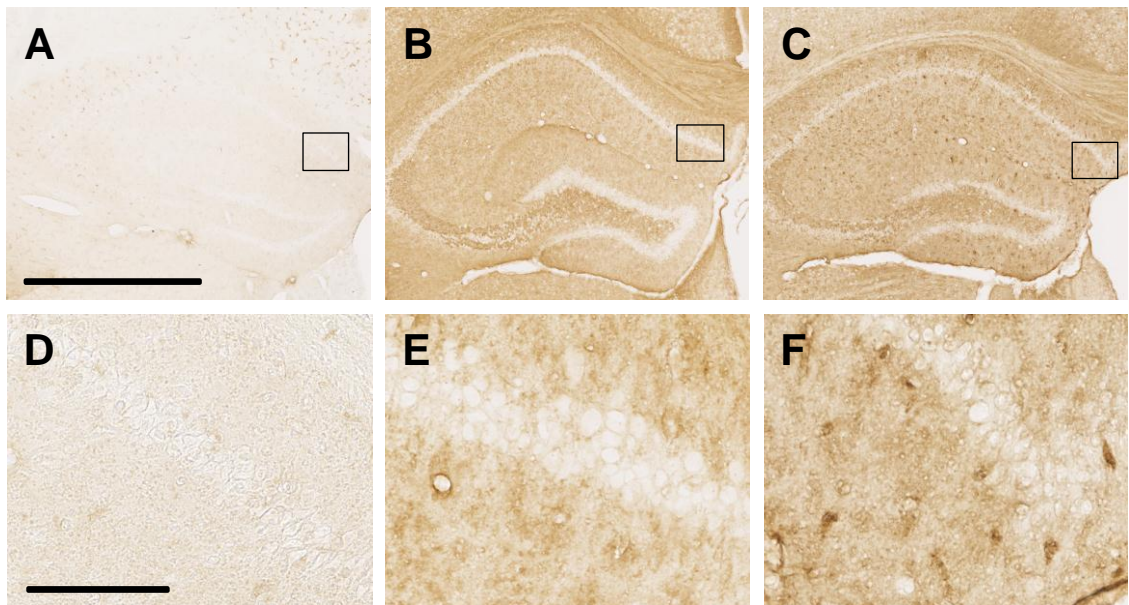
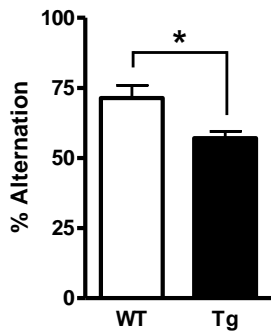


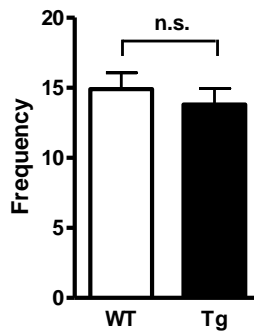
Figure 6. Cognitive deficits in 5-month-old TPR50 mice. Working memory and cognitive function were assessed by the Y-maze test and the novel object recognition test. In the Y-maze test, %alternation was significantly reduced in Tg mice during a 5-minute exploration (A). In the novel object recognition test, exploration of a novel object was evaluated during the retention phase, 24 h after acquisition. Novel object recognition performance is shown as exploration time and novel object preference ratio (B). Data are expressed as mean \pm SEM. * $p \leq 0.05$ by Student's *t*-test, n = 10. n.s., not significant.

A

Spontaneous Alternation

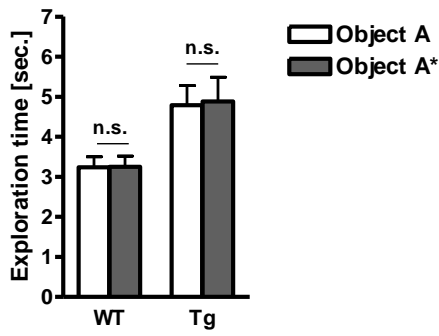


Total Entries

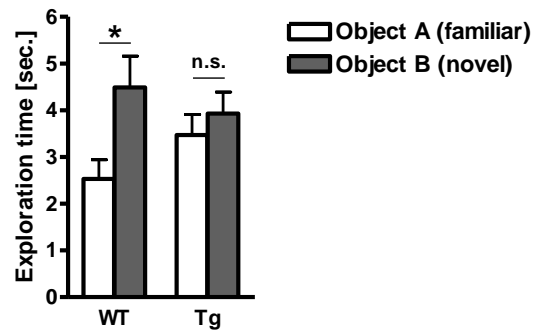


B

Acquisition (duration)



Retention (duration)



Novel object preference ratio

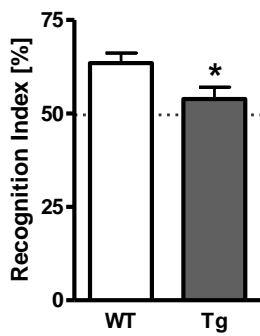


Figure 7. Expression of α -tubulin, acetylated tubulin, kinesin heavy chain (KHC), calbindin, synaptophysin, and β -actin in TPR50 mice. Hippocampal expression of these proteins in TPR50 (Tg) and WT mice at 3, 6, and 9 months of age were examined by Western blotting (A) and quantitative densitometry (B–G). Data are expressed as mean \pm SEM. * $p \leq 0.05$, ** $p \leq 0.01$ by Student's *t*-test, $n = 5$. n.s., not significant.

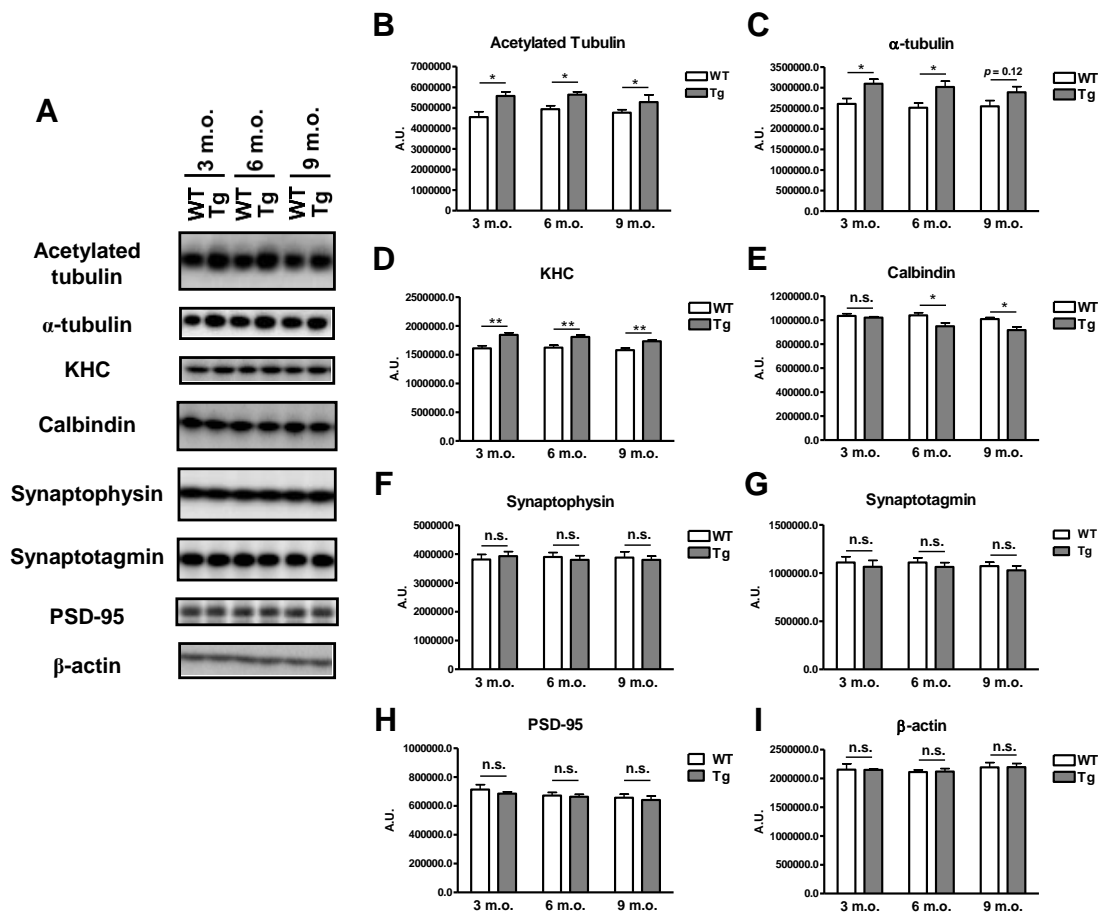


Figure 8. MThyberdynamics in TPR50 mice. *In vivo* MT dynamics measured in the cerebral cortex (A and D), hippocampus (B and E), and cerebellum (C and F) of TPR50 (Tg) and WT mice at 4 (A–C) and 7 (D–F) months of age. Data are expressed as mean \pm SEM. * $p \leq 0.05$, ** $p \leq 0.01$ by Student's *t*-test, $n = 3$. n.s., not significant.

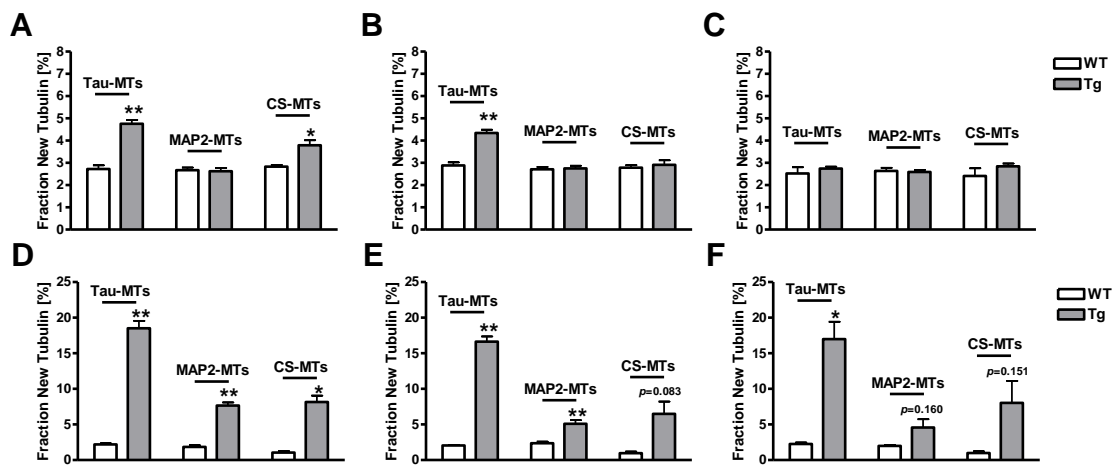
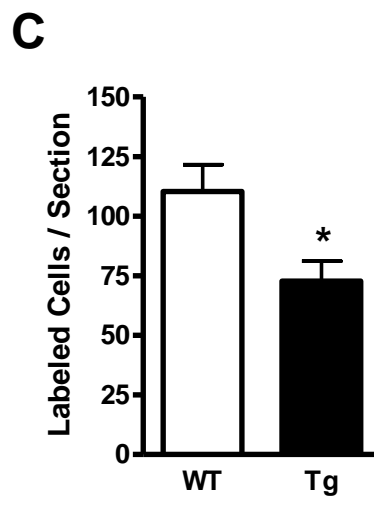
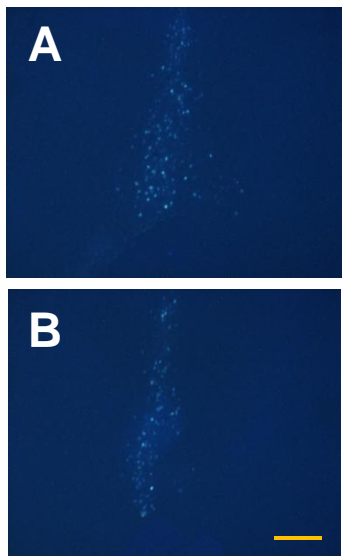
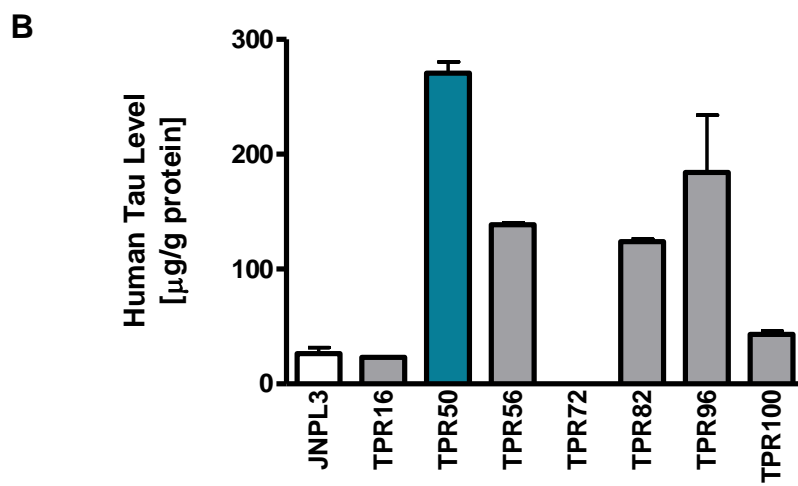
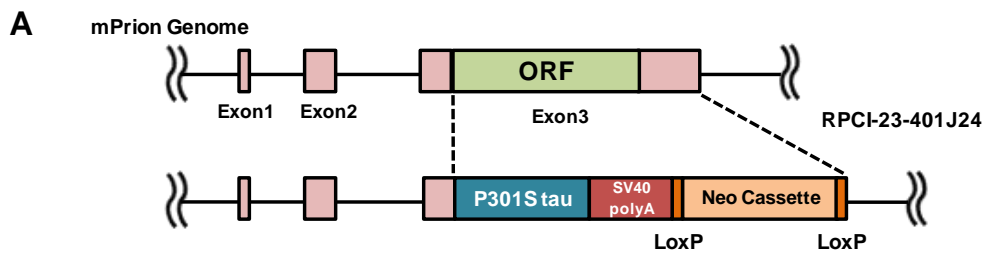


Figure 9. Impaired septohippocampal retrograde transport in TPR50. The retrograde axonal tracer Fluoro-Gold was injected into the right hippocampus of 5-month-old TPR50 (Tg) and WT mice. Three days after injection, labeled neurons in the medial septum were surveyed in WT (A) and Tg (B) mice and counted (C). Data was expressed as mean \pm SEM. * $p \leq 0.05$ by Student's *t*-test, n = 8. Bar = 500 μ m



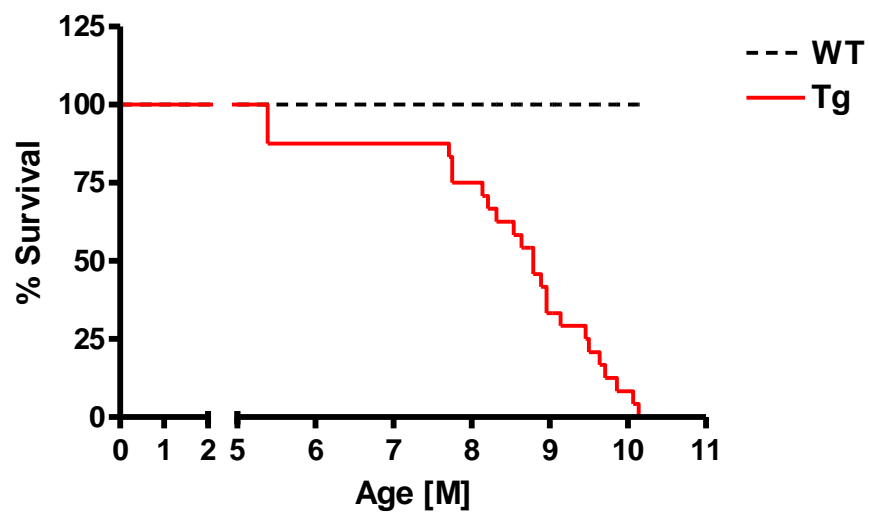
Supplementary Information

Supplementary Figure 1. Generation of the TPR50 mouse. (A) The open reading frame (ORF) of the mouse prion gene in the BAC vector (RPCI-23-401J24) was replaced with the human 4R2N tau gene harboring the P301S mutation and a selection cassette flanked by loxP sequences by ET recombination. Tg mice were generated by microinjection of the vector into oocytes harvested from BDF1 mice. (B) Expression of human tau in the 7 lines obtained (TPR16, 50, 56, 72, 82, 96, and 100). Human tau was measured by ELISA. Data was expressed as mean \pm SEM, n = 3.

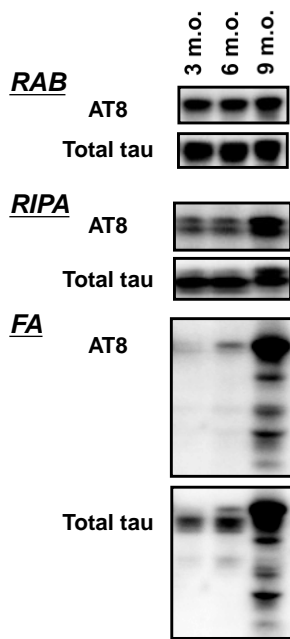
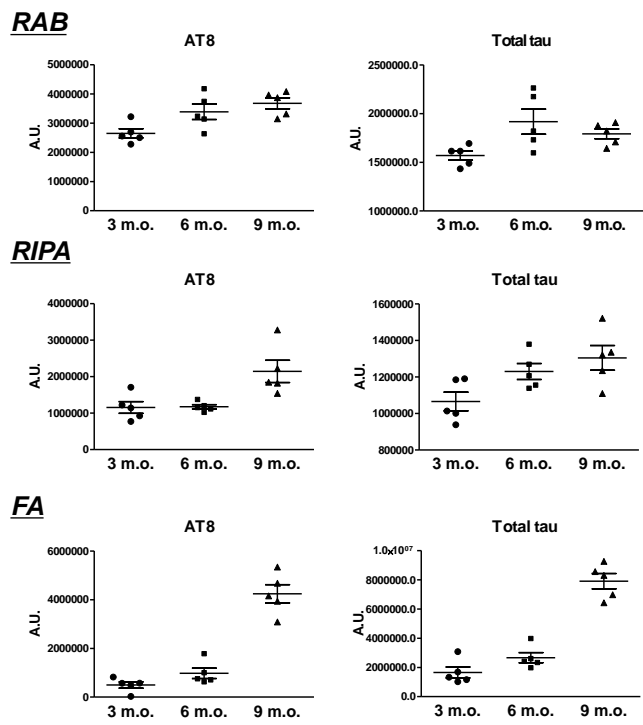


Supplementary Figure 2 Kaplan–Meier curve of time to natural death or required euthanasia of male TPR50 (Tg) and WT mice.

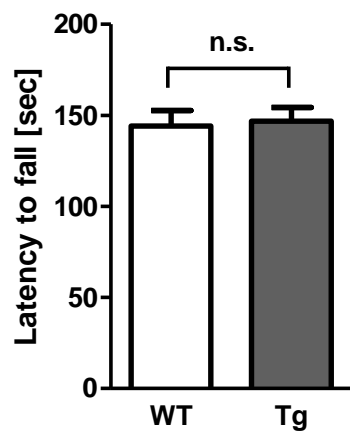
Data are expressed as %survival, n = 24/group.



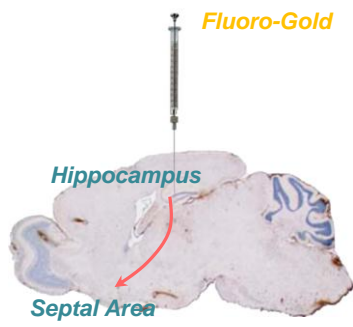
Supplementary Figure 3. RAB-RIPA-FA extraction of tau from the hippocampus of TPR50 mice at 3, 6, and 9 months of age. Each fraction was examined by Western blotting using antibodies against pS202/T205-tau (detected with AT8) and total tau (A) and analyzed by densitometry (B). Data are expressed as the scatter dot plot and mean \pm SEM, n = 5.

A**B**

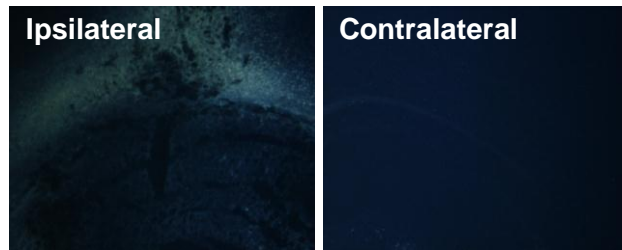
Supplementary Figure 4. Motor phenotype assessed by the rotarod in young TPR50 mice. TPR50 mice and WT mice at 5 months of age were subjected to the rotarod test, and motor function was expressed as latency to fall off the apparatus. Data are expressed as mean \pm SEM and statistically analyzed by Student's *t*-test, n = 8. n.s., not significant.



Supplementary Figure 5. Experimental scheme for evaluation of retrograde axonal transport in the septohippocampal pathway. Fluoro-Gold is injected into the hippocampus, the target of septal cholinergic neuron projections (*left*). The dye was diffused in the ipsilateral site of injection while the contralateral site was intact. Cells labeled by the dye transported to the septum in a retrograde manner were detected in the septum (*right*). MS, medial septal nucleus.



Hippocampus



Bregma -2.30 mm

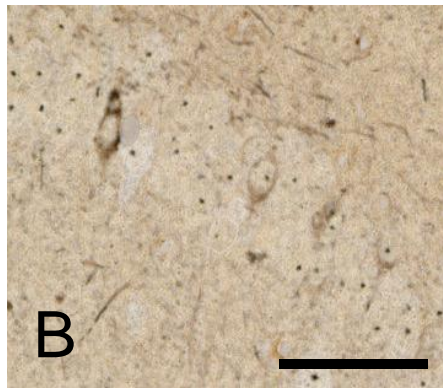
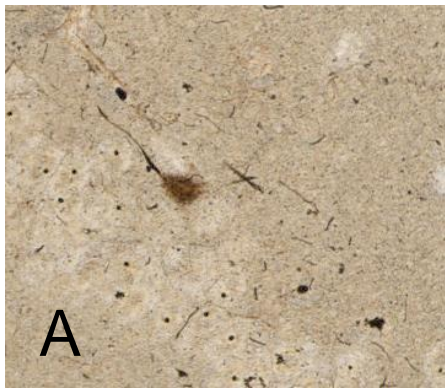
Septal Area



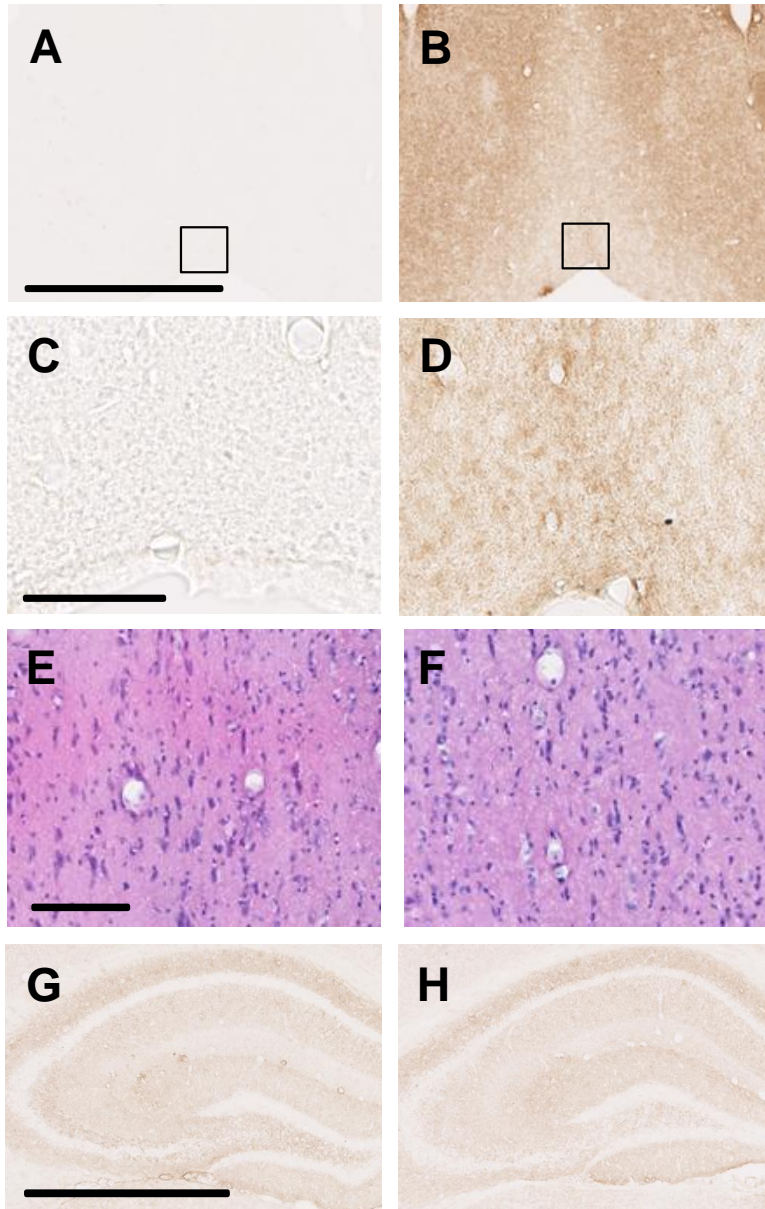
Bregma 1.10 mm

Supplementary Figure 6. Tangle-like pathology in 9-month-old TPR50 mice examined by Bielschowsky silver staining. (A) Sagittal section, (B) coronal section of hippocampus.

Bar = 100 μ m



Supplementary Figure 7. Histological analysis of 5-month-old TPR50 mice. Septal sections were examined by immunohistochemistry using a human tau antibody (HT7) (A–D) and HE staining (E and F). C and D are magnified regions of A and B, respectively. Hippocampal sections were examined by immunohistochemistry using antibodies for synaptophysin (G and H). A, C, E, and G: 5-month-old WT mice, B, D, F, and H: 5-month-old TPR50 mice. Bar = 1 mm (A, B, E, and F); 100 μ m (C, D, E, and F).



Part II

A Novel Glycogen Synthase Kinase-3 Inhibitor

2-methyl-5-(3-{4-[(S)-methylsulfinyl]phenyl}-1-benzofuran-5-yl)-1,3,4-oxadiazole
(MMBO) Decreases Tau Phosphorylation and Ameliorates Cognitive Deficits in a
Transgenic Model of Alzheimer's Disease

Abstract

AD is a neurodegenerative disorder leading to a progressive loss of cognitive function and is pathologically characterized by senile plaques and NFTs. GSK-3 is involved in AD pathogenesis. GSK-3 is reported not only to phosphorylate tau, a major component of NFTs, but also to regulate the production of A β , which is deposited in senile plaques. Therefore, pharmacological inhibition of GSK-3 is considered an attractive therapeutic approach. Here, I report the pharmacological effects of a novel GSK-3 inhibitor, MMBO, which displays high selectivity for GSK-3 and brain penetration following oral administration. MMBO inhibited tau phosphorylation in primary neural cell culture and also in normal mouse brain. When administered to a transgenic mouse model of AD, MMBO significantly decreased hippocampal tau phosphorylation at GSK-3 sites. Additionally, chronic MMBO administration suppressed tau pathology as assessed by AT8-immunoreactivity without affecting A β pathology. Finally, in behavioral assessments, MMBO significantly improved memory and cognitive deficits in the Y-maze and in novel object recognition tests in the transgenic AD mouse model. These results indicate that pharmacological GSK-3 inhibition ameliorates behavioral dysfunction with suppression of tau phosphorylation in an AD mouse model, and that MMBO might be beneficial for AD treatment.

Introduction

AD is a neurodegenerative disorder characterized by a progressive deterioration in cognitive function and memory and has two pathological hallmark lesions: senile plaques and NFTs. These pathological features are comprised of the small peptide, A β and the MT-associated protein, tau, which is hyperphosphorylated at specific sites (Grundke-Iqbal et al., 1986; Friedhoff et al., 2000). Hyperphosphorylation of tau is thought to result in its pathological aggregation with a contribution from several kinases such as GSK-3 β (Sperber et al., 1995) and cyclin-dependent kinase 5 (CDK5) (Cruz and Tsai, 2004).

GSK-3 β is reported to phosphorylate tau and affect MT rearrangement *in vitro* (Lovestone et al., 1996; Wagner et al., 1996) and also to be associated with the formation of tau oligomeric fibrils (Sato et al., 2002; Ishizawa et al., 2003; Noble et al., 2003) and NFTs in AD (Pei et al., 1997, 1999). In addition, overexpression or activation of GSK-3 β in mice induces AD-like symptoms such as tau hyperphosphorylation and cognitive deficits (Lucas et al., 2001; Hernández et al., 2002; Engel et al., 2006; Wang et al., 2008). These phenotypes are completely reversed after silencing of a GSK-3 β transgene with the Tet-off system (Engel et al., 2006). These reports indicate that inhibition of GSK-3 β can be a potent therapeutic approach for AD. In fact, some reports show that inhibition of GSK-3 β with small molecules including lithium, a medication for bipolar disorder, decreases tau phosphorylation and improves neuronal abnormalities such as motor deficits in JNPL3 mice (Noble et al., 2005; Le Corre et al., 2006).

Other reports imply that GSK-3 α and β may also affect A β production. GSK-3 α regulates A β production via γ -secretase (Phiel et al., 2003), and lithium reduces A β

plaque pathology in APP Tg mice (Su et al., 2004). Moreover, dominant-negative (DN)-GSK-3 β Tg mice crossed with APP Tg mice show reduced APP phosphorylation and A β plaque pathology (Rockenstein et al., 2007). These results indicate that GSK-3 inhibition might represent a beneficial strategy for lowering A β as well as for inhibiting tau phosphorylation.

So far, lithium has been widely used as a GSK-3 inhibitor in many pharmacological studies. Lithium inhibits GSK-3 β activity both directly (Klein and Melton, 1996; Phiel and Klein, 2001) and indirectly (Chalecka-Franaszek and Chuang, 1999; Zhang et al., 2003). However, lithium is known to inhibit not only GSK-3 but also other important kinases such as casein kinase 2 (CK2), mitogen-activated protein kinase activated protein kinase 2 (MAPKAP-K2) and p38-regulated/activated kinase (PRAK) (Davies et al., 2000). Therefore, I conducted this study in order to clarify potential of GSK-3 as a therapeutic target for neurodegenerative diseases.

Here, I report a further investigation into the pharmacological inhibition of GSK-3 using a novel, selective inhibitor in 3xTg-AD mice. The inhibitor is highly selective for GSK-3, and also orally effective *in vivo* (Saitoh et al., 2009a and 2009b). Triple Tg-AD mice express human mutant APP_{swe}, PS1_{M146V} and tau_{P301L} and develop both A β plaques and NFTs in an age- and region-dependent manner (Oddo et al., 2003). In addition, they also suffer age-dependent deficits in cognition and learning behavior (Billings et al., 2005; Clinton et al., 2007; Gimenez-Llort et al., 2007). Therefore, using these mice as a model of AD, we examined the putative therapeutic effects of a selective GSK-3 inhibitor on AD-like pathology and associated behaviors.

Materials and Methods

Animals

The 3xTg-AD mice, originally developed by Oddo and colleagues (2003), were bred in our laboratories and were used in this study. The 3xTg-AD mice were derived by co-microinjected human APP with the Swedish mutation (KM670/671NL) and human tau with the P301L mutation (both regulated under the Thy1.2 promoter) into single-cell embryos harvested from homozygous mutant PS1^{M146V} knockin (PS1-KI) mice. The background of the PS1-KI is a hybrid 129/C57BL6 used as a NonTg control. The JNPL3 and wild type control mice were purchased from Taconic (Hudson, NY). JNPL3 mice express human tau with a P301L mutation under the mouse prion promoter (MoPrP) and their background is C57BL/DBA/SW (Lewis et al., 2000). Mice were housed in groups on 12 h light/dark cycles and were provided *ad libitum* access to food and water. All animals were maintained and sacrificed according to the guidelines of the Takeda Experimental Animal Care and Use Committee.

Chemical treatment

A GSK-3 inhibitor, 2-methyl-5-(3-{4-[(S)-methylsulfinyl]phenyl}-1-benzofuran-5-yl)-1,3,4-oxadiazole (MMBO), was synthesized in our laboratories (Saitoh et al., 2009a). The compound was dissolved in DMSO at a concentration of 30 mM and was applied to cells after dilution with medium at the indicated concentrations. In the *in vivo* experiments, MMBO was reconstituted in 0.5% methylcellulose and administered orally at the indicated doses. To evaluate tau pathology, MMBO was administered for 22 days to 13-month-old 3xTg-AD mice (p.o., b.i.d.). To assess APP/A β metabolism, MMBO was

administered for 33 days to 11-month-old 3xTg-AD mice (p.o., b.i.d.). Behavioral tests were also performed in these animals. At a treatment time of 17 days and 25 days, Y-maze tests and novel object recognition tests were performed, respectively.

Kinase assay

Human GSK-3 α and GSK-3 β were purchased from Millipore Corp. (Bedford, MA). The kinase assay was performed according to methods previously reported (Uno et al., 2009). Briefly, the reaction was conducted in 25 mM HEPES (pH 7.5), 10 mM magnesium acetate, 1 mM dithiothreitol, and 0.01% BSA. Compounds were dissolved in DMSO and then applied at the indicated doses in each reaction. The final amount of enzyme and substrate were optimized to the following: 40 ng/well of enzyme and 400 ng/well of GSK-3 substrate peptide (Millipore Corp.). All kinase reactions were started by addition of the ATP solution (final concentration 500 nM), and incubations occurred for 45 minutes at room temperature. The reactions were terminated by the Kinase-Glo reagent containing EDTA (50 μ L/well, Promega Corp., Madison, WI, USA). Ten minutes after the addition of the Kinase-Glo reagent, luminescence was measured.

Antibodies

The following antibodies were used in this study: AT8 (Innogenetics, Ghent, Belgium), Ab-3 (Thermo Fisher Scientific, Fremont, CA, USA), pS199-tau (Invitrogen, Carlsbad, CA, USA), pS214-tau (Invitrogen), HT7 (Innogenetics), pT205-tau (Invitrogen), pS396-tau (Invitrogen), AT270 (Innogenetics), AT180 (Innogenetics) and β -actin (Sigma, St. Louis, MO). Antibodies for A β used in this study (BNT77, BA27, and BC05) have been previously described (Asami-Odaka et al., 1995).

Rat primary culture and tau phosphorylation inhibition assay

Primary cortical neurons were prepared from E17 SD rat embryos (Japan Slc, Shizuoka, Japan) using a papain-containing nerve cell dispersion kit (Sumitomo Bakelite, Akita, Japan). Isolated cells were suspended in nerve cell culture medium (Sumitomo Bakelite). The cells were seeded on poly-D-lysine/laminin coated plates (BD, Franklin Lakes, NJ, USA) under 5% CO₂ at 37°C for 4 DIV to estimate tau phosphorylation. In the assay, cells were treated with MMBO at the indicated concentrations for 2 hours, then fixed with 4% paraformaldehyde (Wako, Osaka, Japan) for 30 minutes at room temperature, and finally treated for 1 hour with 1.5% BSA and 0.1% TritonX-100 in PBS at room temperature. Neurons were then immunostained with primary antibodies against phosphorylated tau (AT8, 1: 200 dilution) or total tau (Ab-3, 1: 500 dilution) and then labeled with Alexa-conjugated secondary antibodies (Invitrogen). Images were captured using a TE2000-U (Nikon, Tokyo, Japan).

A β measurement by ELISA

Hippocampi were isolated from animals and immediately frozen on dry ice and stored at -80°C until assay. Samples were homogenized in ice-cold Tris-extraction buffer (50 mM Tris-HCl, pH 7.2, 200 mM sodium chloride, 2% protease-free bovine serum albumin, and 0.01% sodium merthiolate) containing protease inhibitor cocktails (Roche, Basel, Switzerland). After centrifugation at 15,000 g for 15 minutes, the supernatants were subjected to two-site sandwich ELISA to measure amounts of soluble A β . For assessment of insoluble A β , the pellets were homogenized in guanidine extraction buffer (5 M guanidine, 50 mM Tris-HCl (pH 7.2)) and centrifuged at 15,000 g for 15 minutes.

The supernatants were diluted with 19-fold Tris-extraction buffer and subjected to ELISA. A β 40 or A β 42 was quantified by two-site sandwich ELISA using BNT77, which recognizes A β 11-16, as a capture antibody and BA27-HRP or BC05-HRP as a detector antibody, respectively, as described previously (Asami-Odaka et al., 1995).

Western blotting

Hippocampi isolated from mice were homogenized in RIPA extraction buffer (50 mM Tris-HCl, 5 mM EDTA, 1 mM EGTA, 100 mM NaCl, 1% NP-40 and 2.5% sodium deoxycholate, pH7.5) supplemented with protease inhibitors (1.37 mg/L pepstatin A, 25 KIU/mL aprotinin, 1 nM microcystin LR, 1 nM MG115, 40 nM leupeptin and 100 nM 4-(2-aminoethyl)benzenesulfonyl fluoride HCl) and phosphatase inhibitors (30 mM NaF, sodium diphosphate, 2 mM sodium orthovanadate). The homogenate was centrifuged at 10,000 g for 10 minutes and the supernatant was taken as the soluble fraction. Protein concentration was determined using the BCA assay kit (Pierce, Rockford, IL). Equal amounts of protein (1-10 μ g depending on the protein of interest) were separated by SDS-PAGE on a 10% polyacrylamide gel, then electrophoretically transferred to 0.45 μ m poly-vinylidene difluoride membranes (Millipore) and blocked for 1 hour in BlockAce (DS Pharma Biomedical, Osaka, Japan). After blocking, membranes were probed with primary antibodies followed by labeling with horseradish peroxidase-coupled secondary antibodies (Amersham, Piscataway, NJ), and then visualized by a chemiluminescence reagent (Immunostar; Wako) using a LAS1000 imaging system (Fujifilm, Tokyo, Japan). Quantitative densitometric analyses were performed with Image Gauge (Fujifilm). Values presented are derived from densitometry arbitrary units (AU).

Statistical analysis

Data are expressed as mean \pm SEM and were analyzed by the one-tailed Williams' test, and $p = 0.025$ or lower was considered significant. For comparisons between vehicle-treated WT mice and vehicle-treated Tg mice, Student's t -tests were performed using $p = 0.05$ or lower as a significant level. Student's t -tests were also used for comparisons in the novel object recognition test. Analyses were performed with SAS system 8 (SAS Institute, Cary, NC, USA)

Results

MMBO, a novel GSK-3 inhibitor, decreased tau phosphorylation *in vitro* and *in vivo*

In this study, I used a novel GSK-3 inhibitor, MMBO. The chemical structure of MMBO is shown in Figure 10. This compound displays high selectivity for GSK-3 out of various kinases such as cyclin-dependent kinase 5 (CDK5), extracellular signal-regulated kinase 1 (ERK1), and Jun N-terminal kinase (JNK), although selectivity for GSK-3 α vs. GSK-3 β is unknown (Saitoh et al., 2009b). Therefore, we first evaluated the inhibitory activity of MMBO on GSK-3 α/β . As shown in Table 1, MMBO inhibited both GSK-3 α and β to a similar extent with an IC₅₀ of 37 and 53 nM, respectively. Lithium, a well-known GSK-3 inhibitor, also inhibited both subtypes, but its inhibitory activities were much weaker compared to MMBO.

To examine whether MMBO decreases tau phosphorylation in neural cells, rat primary neural cell cultures were treated with MMBO. The amount of phosphorylated tau was assessed by immunostaining (Figures 11A-I) or Western blotting (Figures 11J and K) with AT8 antibody, which recognizes tau phosphorylated at S202 and T205. While DMSO-treated neurons showed AT8-positive immunoreactivity identical to total tau stained with Ab-3 (Figures 11A-C), MMBO-treated cells showed a reduction of AT8 immunostaining without any changes in total tau (Figures 11D-I). Results of Western blotting and quantitative analyses supported these observations (Figures 11J and K).

Next, I examined the brain penetration and tau phosphorylation inhibitory activity of MMBO *in vivo*. MMBO was administered to C57BL/6N mice and its brain concentration was measured. Area under the curve (AUC) concentration values from 0-24 hours after administration in the brain and plasma were 734.2 ng h/g and 457.4 ng h/mL,

respectively, when orally dosed at 3 mg/kg, indicating that MMBO is able to penetrate the brain (Table 2A). Time course profiles of concentrations in brain and plasma were similar, and maximum concentrations were seen 30 minutes after administration (Table 2B). Tau phosphorylation in the hippocampus was assessed by pT205-tau and total tau antibodies (Figures 12A and B). Tau phosphorylation in MMBO-treated mice was decreased 30 minutes after administration, and then returned to baseline level by 4 hours. The time course profile of tau phosphorylation reduction was well correlated with drug levels.

Effects of MMBO on tau phosphorylation and pathology in 3xTg-AD mice

To evaluate the effects of MMBO on tau phosphorylation in an AD animal model, we administered the drug to 3xTg-AD mice. Triple Tg-AD mice reveal AD-like tau pathology and memory impairments without the motor deficits seen in other tau transgenic mice, such as JNPL3 mice (Lewis et al., 2000). Therefore, 3xTg-AD mice were thought to be the most suitable for the evaluation of MMBO. In addition, human tau expression in 3xTg-AD mice varied less compared to JNPL3 mice (Supplementary Figure 8), suggesting that 3xTg-AD mice are useful for pharmacological studies of tau pathology.

MMBO was administered orally to the 3xTg-AD mice at doses of 3 and 10 mg/kg. Tau phosphorylation at T181, S199, T205, S202/T205, T231, and S396, residues reported to be GSK-3 β -sensitive sites, were significantly reduced by MMBO in a dose-dependent manner, while total tau levels were comparable among all groups (Figure 13). Tau phosphorylation at S214 was not inhibited by MMBO (Figures 13A and F), indicating that this phosphorylation site might not be affected directly by GSK-3, as reported in

previous *in vitro* studies (Liu et al., 2002; Wang et al., 2007).

To assess the effects of MMBO on tau pathology, MMBO was administered to 13-month-old 3xTg-AD mice for 3 weeks. Consistent with a previous report mentioning that AT8-reactive neurons become apparent between 12 to 15 months of age (Oddo et al., 2003), AT8-positive phosphorylated tau and HT7-positive total human tau both pathologically accumulated in the CA1 of 3xTg-AD mice (Figures 14A, D, G and J). The AT8-positive pathology was reduced by treatment with MMBO in a dose-dependent manner (Figures 14A-F). HT7-positive total tau in MMBO-treated animals only showed a trend towards reduction when compared to vehicle-treated mice (Figures 14G-L).

Effects of MMBO on APP metabolism in 3xTg-AD mice

As described above, previous studies also show that GSK-3 regulates A β production. Therefore, I examined whether MMBO affects APP metabolism and A β pathology in 3xTg-AD mice. MMBO was administered to 11-month-old 3xTg-AD mice (at which time A β pathology is considered to be forming) for 5 weeks. Subsequently, Tris-soluble and insoluble A β levels in the hippocampus were measured. MMBO at 1 and 3 mg/kg did not change A β levels (Figures 15A and B). A β deposits in hippocampi evaluated by immunohistochemistry using the A β antibody were also not different between vehicle- and MMBO-treated animals (Figure 15C). Since previous studies suggested that GSK-3 regulates phosphorylation-dependent A β production (Aplin et al., 1996; Ryder et al., 2003; Su et al., 2004; Rockenstein et al., 2007), APP phosphorylation at Thr688 was examined in the hippocampi of MMBO-treated mice. However, APP phosphorylation was not affected by MMBO treatment (Figure 15D).

Effects of MMBO on cognitive behavior in 3xTg-AD mice

Finally, the effect of MMBO on cognitive behavior was assessed. MMBO was chronically administered to 11-month-old 3xTg-AD mice. Subsequently, Y-maze tests were performed. Spontaneous alternation in the Y-maze primarily depends on hippocampal function and is often used to evaluate short-term memory. Triple Tg-AD mice showed impaired spontaneous alternation performance compared with vehicle-treated WT mice ($p \leq 0.01$) (Figure 16A). Mice treated with MMBO for 17 days increased their spontaneous alternation in a dose-dependent manner ($p \leq 0.025$). Total arm entries were significantly decreased in Tg mice compared to the WT group, but were comparable between vehicle and MMBO treatment groups (Figure 16B). Thereafter, cognitive function was assessed in the novel object recognition test 8 days after the Y-maze (on the 25th day of treatment). During the acquisition phase, all mice explored both objects (objects A and A*) comparably (data not shown). After a 5-hour delay, while the vehicle-treated WT mice showed significant exploration of the novel object (object B) ($p \leq 0.001$), the 3xTg-AD mice treated with vehicle were impaired in their recognition of the novel object as shown in Figure 17. In contrast, MMBO significantly increased the frequency of exploration of the novel object and the recognition index ($p \leq 0.05$). These results indicate that MMBO improved both memory and cognitive function in 3xTg-AD mice.

Discussion

In this study, I examined the therapeutic effects of GSK-3 inhibition with a novel compound, MMBO, which displays good selectivity for GSK-3, bioavailability, and brain permeability (Saitoh et al., 2009b). MMBO decreased tau phosphorylation both *in vitro* and *in vivo*. In 3xTg-AD mice, MMBO significantly reduced tau phosphorylation in a dose-dependent manner at residues regulated by GSK-3 (Figure 13).

Previous studies have shown that GSK-3 inhibitors such as lithium and AR-A014418 decrease tau phosphorylation *in vivo* and suppress tau pathology in JNPL3 mice (Pérez et al., 2003; Noble et al., 2005). MMBO displayed greater *in vivo* efficacy than lithium and AR-A014418 as evaluated in the cold-water stress (CWS) model (data not shown). MMBO also suppressed AT8-positive (phosphorylated tau) pathology and ameliorated cognitive behavioral deficits in 3xTg-AD mice in spite of insignificant changes in HT7-positive (total tau) pathology. This result suggests that MMBO might not drastically suppress tau accumulation but might affect the phosphorylation of intracellular tau, and the effect on intracellular soluble tau might produce the behavioral improvements observed. A similar discovery was reported by Oddo and colleagues (2006), who found that A β immunotherapy in 3xTg-AD mice ameliorated cognitive impairment when reducing both soluble A β and soluble tau, but not insoluble tau. Additionally, some recent reports have shown that soluble tau plays an important role in impaired neural function. In APP Tg mice, soluble tau mediated the excitotoxicity induced by A β (Palop et al., 2007; Roberson et al., 2007). In rTg4510 mice, memory deficits and neuronal cell loss were independent of NFTs (Santacruz et al., 2005). Tau-overexpressing flies also showed progressive neurodegeneration in the

absence of NFTs (Wittmann et al., 2001). Consistent with my observations, these reports could indicate that protection from toxicity induced by soluble tau represents a therapeutic strategy for neurodegenerative diseases including AD, although the toxicity of soluble tau has not been explicitly demonstrated. Additionally, the fact that antibody responders following A β vaccination show a decrease in soluble tau levels in the cerebrospinal fluid (CSF) would seem to provide further evidence of the importance of soluble tau in cognitive function (Gilman et al., 2005).

Recently, Caccamo and colleagues reported the effects of lithium in 3xTg-AD mice (2007). Lithium treatment decreased tau phosphorylation as measured by Western blotting and immunohistochemistry, similar to my results with MMBO, but did not rescue working memory impairments as assessed by the T-maze test. They speculated that a decrease in both soluble A β and soluble tau might be necessary to improve working memory impairments in 3xTg-AD mice, as was found with A β immunotherapy (Oddo et al., 2006). Comparatively, MMBO was able to ameliorate behavioral deficits in 3xTg-AD mice (Figure 17). The reason why MMBO but not lithium improved working memory in 3xTg-AD mice might be based on several differences in experimental procedures and conditions between these studies. One of the differences involves the particular behavioral tasks assessed. In the previous study, the effects of lithium were evaluated in the T-maze, while, as I show here, MMBO was effective in the Y-maze and novel object recognition tests. Although alternation performance is commonly used in both the T-maze and Y-maze as an index of memory, the Y-maze might be more sensitive for the evaluation of GSK-3 β inhibitors. Another difference might relate to the inhibitory activity and specificity of the compounds. MMBO has more specific activity against GSK-3 and greater *in vivo* efficacy compared to lithium. In addition, the ages of

the 3xTg-AD mice used also differed, as Caccamo et al. evaluated 15-month-old mice while I used somewhat younger animals. In this case, there might be a specific, suitable age for behavioral evaluation.

AD is characterized by the presence of A β plaques in addition to tauopathy, and GSK-3 is reported to also regulate A β production. Although previous reports suggested a beneficial effect of GSK-3 inhibition on lowering A β (as mentioned above), in the current study, pharmacological inhibition of GSK-3 with MMBO did not significantly change A β levels or A β plaque formation (Figures 15A-C). Additionally, APP phosphorylation was not affected by MMBO treatment (Figure 15D). In a separate series of experiments, acutely administered MMBO did not decrease APP phosphorylation or soluble A β 40 or A β 42 in C57BL/6N mice, although slight A β -lowering effects separate from cytotoxicity could be observed *in vitro* (data not shown). Taken together, the therapeutic effects of MMBO as seen in behavioral tests might be produced via the inhibition of tau phosphorylation but not via the lowering of A β . However, further studies will be required to produce a definitive answer.

The current study shows that administration of MMBO, which is a highly selective and potent GSK-3 inhibitor, leads to cognitive improvement in an AD mouse model. Previous reports have shown that lithium ameliorates behavioral deficits in animal models of cognitive decline, but lithium does not display a strong inhibitory activity or specificity for GSK-3 compared with MMBO. Additionally, no obvious clinical effects of lithium were observed in AD patients (Hampel et al., 2009). In this human study, GSK-3 activity in lymphocytes was not affected by lithium, and therefore it is possible the administered dose might not have been sufficient for GSK-3 inhibition. Thus, the use of a stronger or more selective GSK-3 inhibitor like MMBO may be more advantageous as

an AD therapy. In conclusion, pharmacological GSK-3 inhibition and the resultant decrease in tau phosphorylation may represent a valid therapeutic strategy for AD.

Tables and Figures

Table 1. Comparison of MMBO and lithium on inhibition of GSK-3 α and β activity.

	GSK-3α	GSK-3β	
MMBO	37	53	
Lithium	41 x 10⁶	71 x 10⁶	[nM]

Table 2. Single-dose pharmacokinetic profiles of MMBO in mice following oral (3 mg/kg) administration.

A

	Brain	Plasma
C_{max} (ng/g or ng/mL)	579.8	353.9
T_{max} (h)	0.50	0.50
AUC_{0-24h} (ng·h/g or ng·h/mL)	734.2	457.4
MRT (h)	1.09	1.13

B

Time (h)	Brain [ng/g]	Plasma [ng/mL]
	Mean (S.D.)	
0.25	409.4 (85.6)	246.7 (49.2)
0.5	579.8 (50.3)	353.9 (29.5)
1	334.6 (93.4)	201.5 (64.7)
2	80.6 (22.5)	58.2 (18.9)
4	14.2 (12.3)	7.2 (6.3)
8	0	0.3 (0.6)
24	0	0

Figure 10. Chemical structure of MMBO

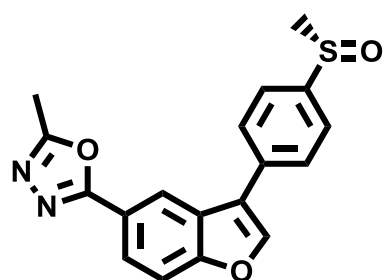


Figure11. Effects of MMBO on tau phosphorylation in rat primary neurons detected by AT8. Rat primary cortical neurons at DIV4 were treated with MMBO at 10 and 30 μ M for 2 hours. MMBO inhibited intracellular tau phosphorylation (*arrowheads*) in a concentration-dependent manner. Phosphorylated tau (A, D, and G) and total tau (B, E, and H) were immunostained by AT8 and Ab-3, respectively. Merged images are shown in C, F, and I. Bar = 20 μ m. Western blotting with AT8 and Ab-3 was also performed (J), and % change from DMSO treated cells was quantified (K).

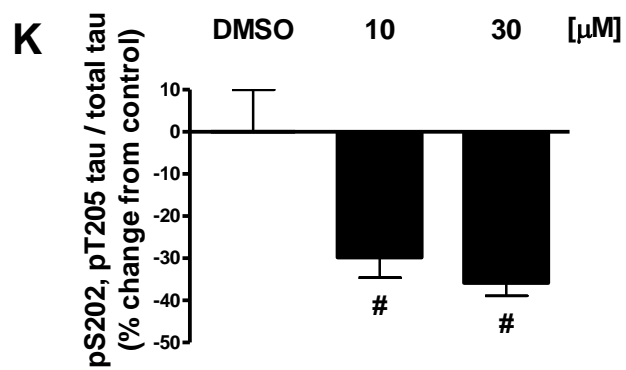
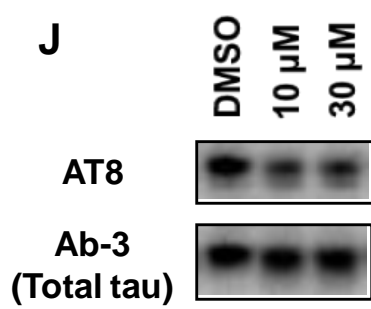
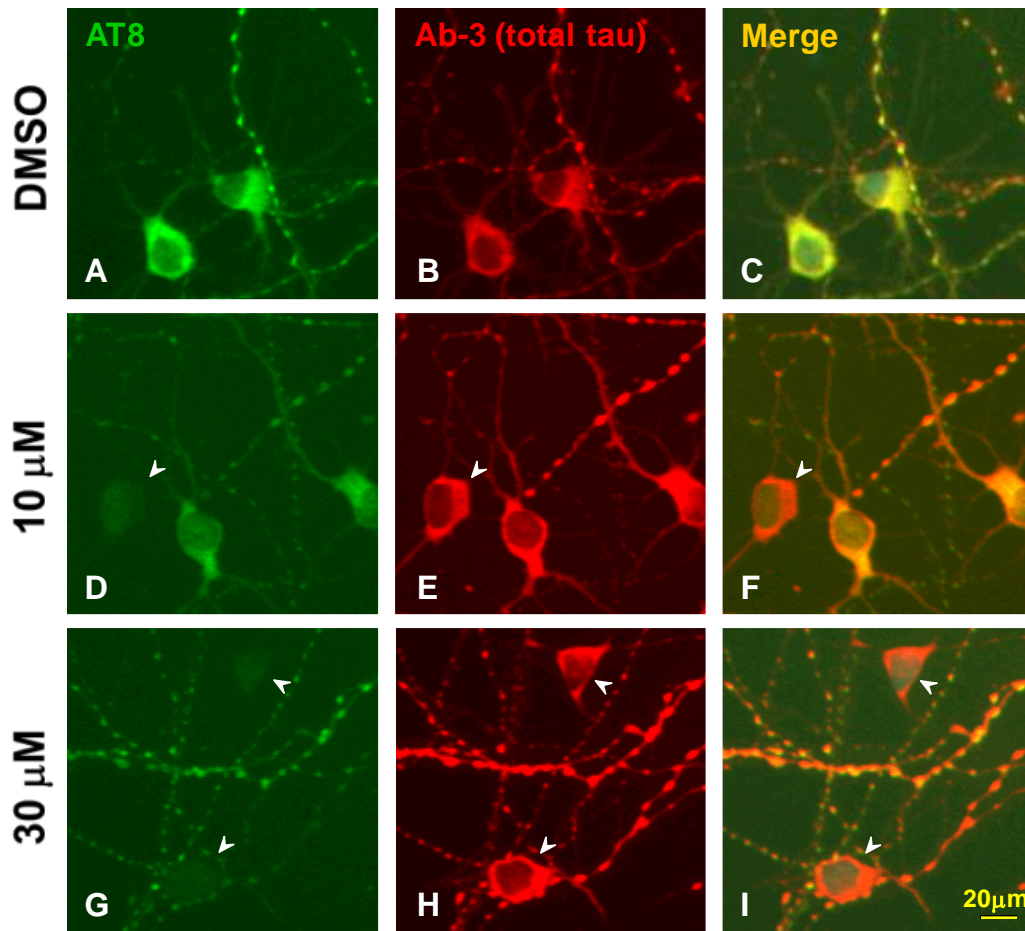
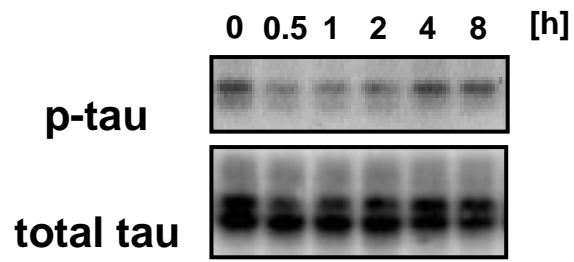


Figure12. Effects of MMBO on tau phosphorylation *in vivo*. Phosphorylated tau in the hippocampus was evaluated at the indicated time (0.5, 1, 2, 4 and 8 hours) after the compound was administered at 10 mg/kg. Tau phosphorylation was analyzed by immunoblot (A) and measured quantitatively (B). Data were expressed as mean \pm SEM, n = 5.

A



B

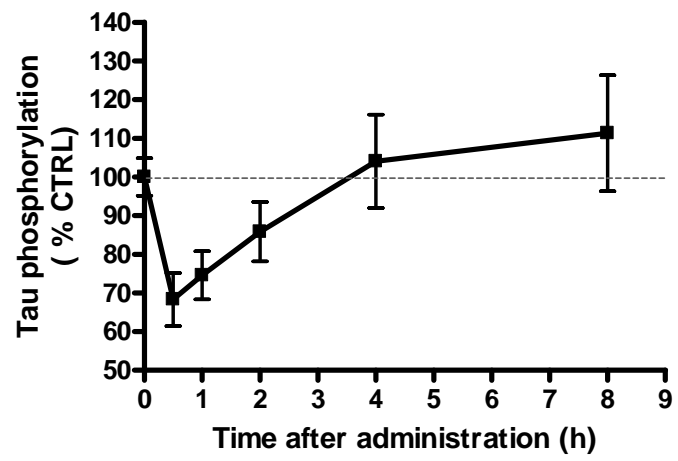


Figure13. Effects of MMBO on tau phosphorylation in 3xTg-AD mice. Vehicle or MMBO at 3 and 10 mg/kg were administered, and 30 minutes after administration phosphorylated tau (pT181-, pS199-, pT205-, pS202/pT205-, pS214-, pT231-, and pS396-tau) in the hippocampus was surveyed by Western blotting (A). Each phosphorylation ratio to total tau is shown as % change from vehicle-treated animals (B-H).

Data were expressed as mean \pm SEM (B-H) and analyzed by a one-tailed Williams' test (vs. vehicle, # $p \leq 0.025$), n = 10.

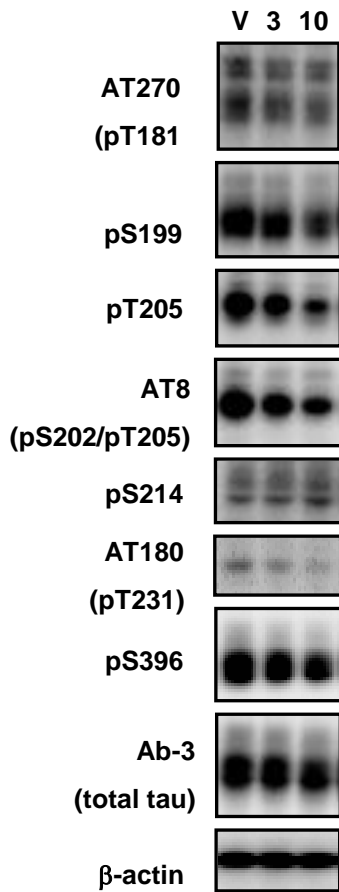
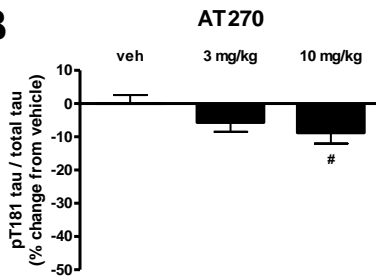
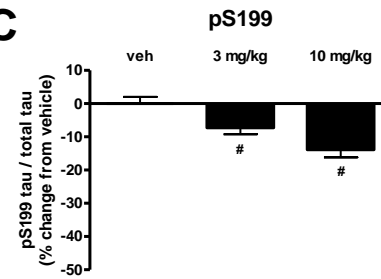
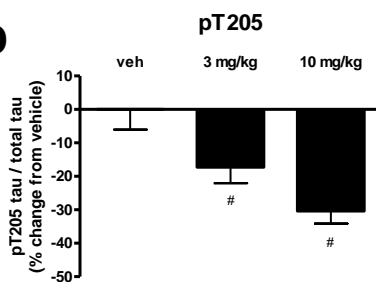
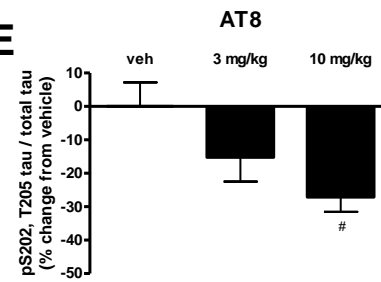
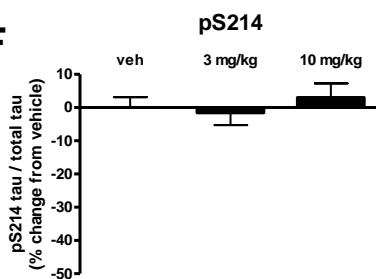
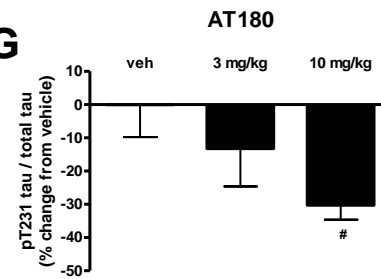
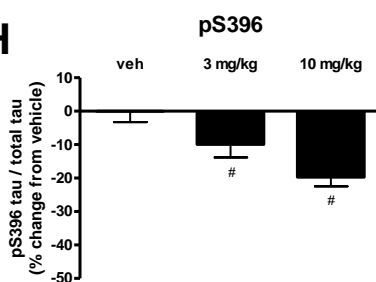
A**B****C****D****E****F****G****H**

Figure14. Effects of MMBO on NFT-like tau pathology in CA1 pyramidal cells of 3xTg-AD mice. Vehicle or MMBO (1 and 3 mg/kg, b.i.d.) was administered to 13-month-old 3xTg-AD mice for 3 weeks. Hippocampi were immunohistochemically stained with AT8 (A-F) or HT-7 (G-L) and then counterstained with hematoxylin. D-F and J-L are magnified images of A-C and G-I, respectively. A, D, G, and J: vehicle, B, E, H, and K: 1 mg/kg, C, F, I, and L: 3 mg/kg. Bar = 300 μ m.

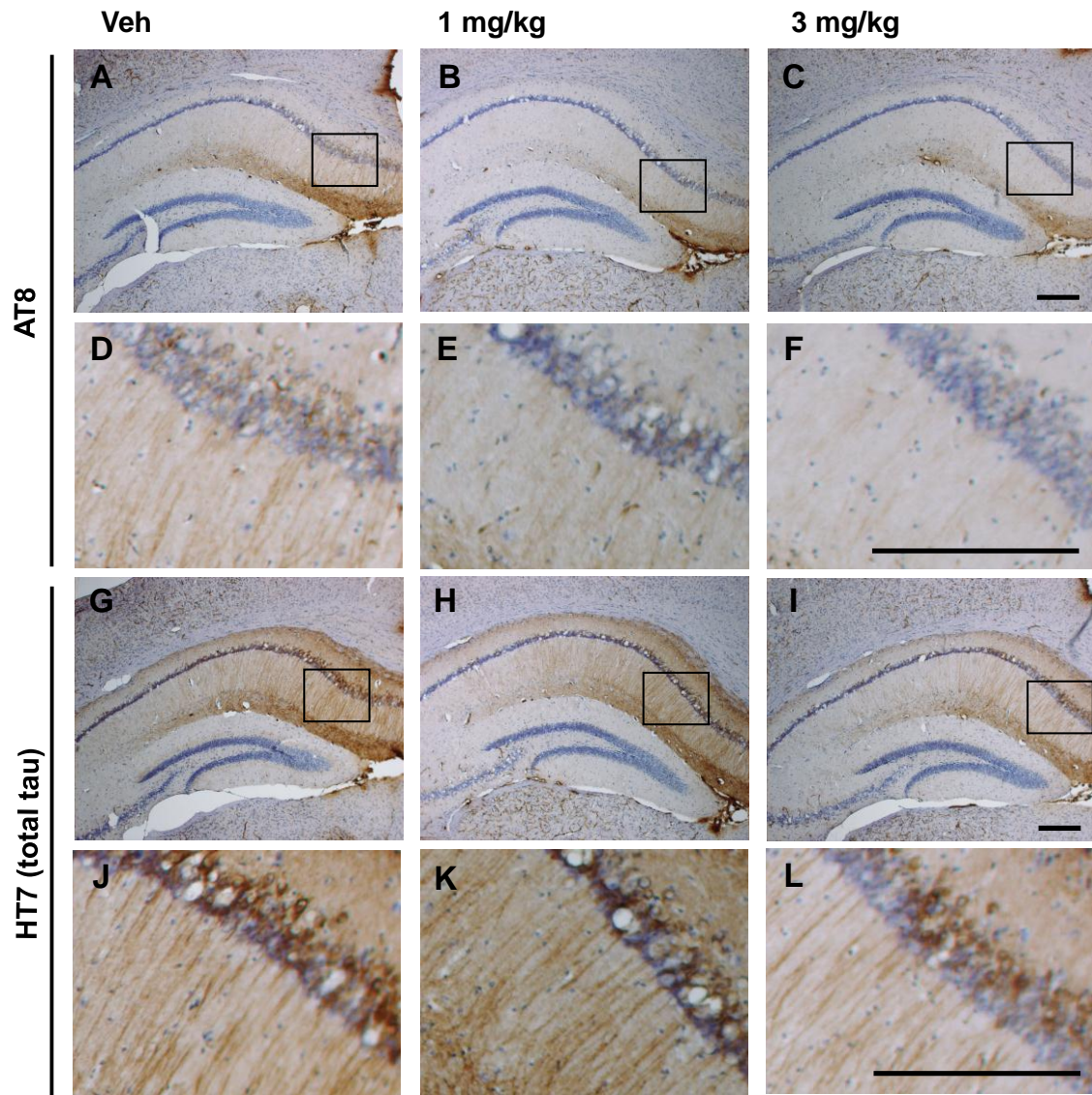


Figure15. Effects of MMBO on APP metabolism and A β pathology. Vehicle or MMBO (1 and 3 mg/kg, b.i.d.) was administered to 11-month-old 3xTg-AD mice for 1 month. Tris-soluble A β (A) and insoluble A β (B) in hippocampi were measured by ELISA. Hippocampi were also immunohistochemically stained with 6E10 (C). APP phosphorylation at T688 was assessed by Western blotting, and then analyzed quantitatively (D). Phosphorylation ratio to total APP is shown as % control. Data were expressed as mean \pm SEM and analyzed by one-tailed Williams' test (vs. vehicle, # $p \leq 0.025$), n = 7.

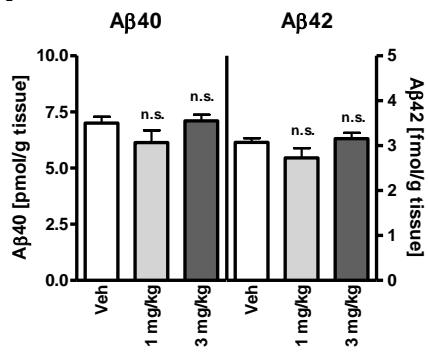
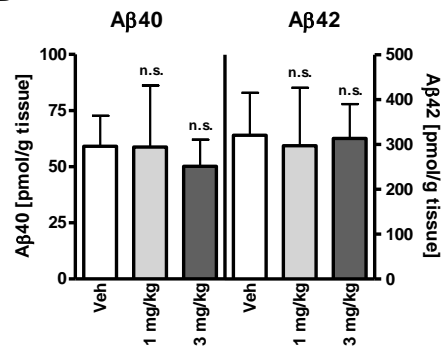
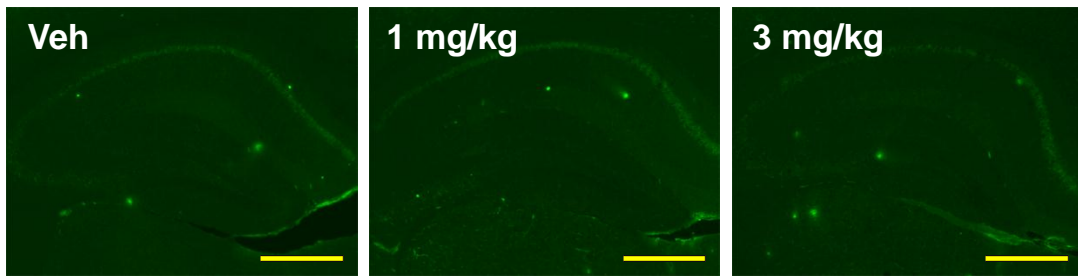
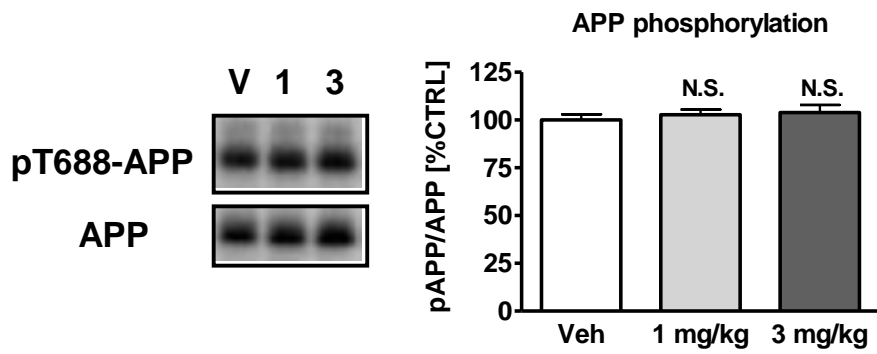
A**B****C****D**

Figure16. Behavioral improvement in the Y-maze after MMBO administration in 3xTg-AD mice. MMBO (1 and 3 mg/kg, b.i.d) or vehicle was administered for 16 days, 30 minutes prior to the Y-maze test. Data are presented as % alternation rate (A) and total frequency of arm entries (B) during an 8-minute exploration. Data were expressed as mean \pm SEM and analyzed statistically as follows: Student's *t*-test (WT vs. Tg, * $p \leq 0.05$, ** $p \leq 0.01$) and one-tailed Williams' test (vs. vehicle, # $p \leq 0.025$), $n = 10$.

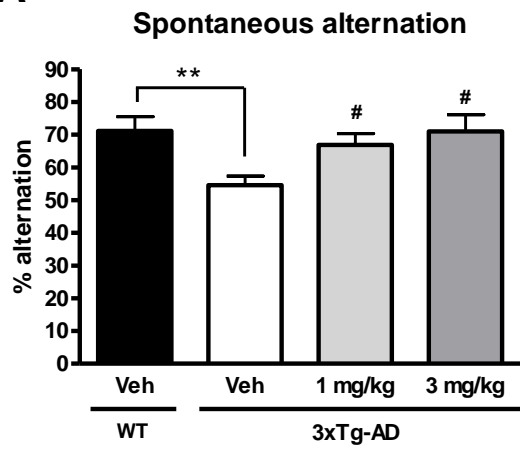
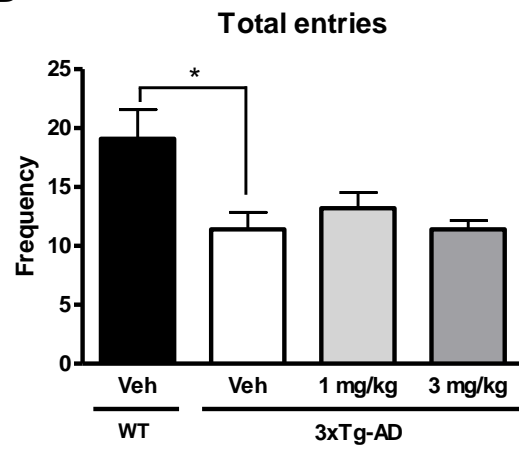
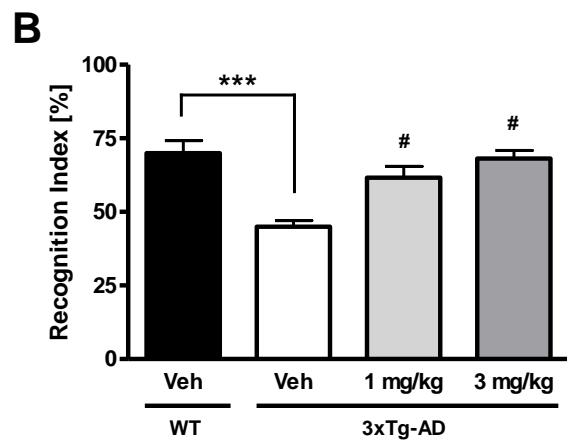
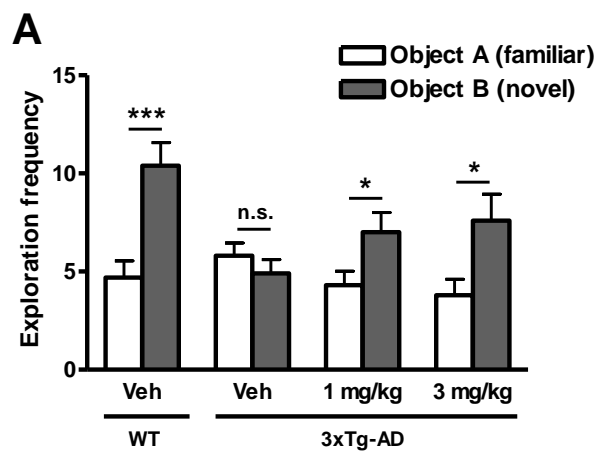
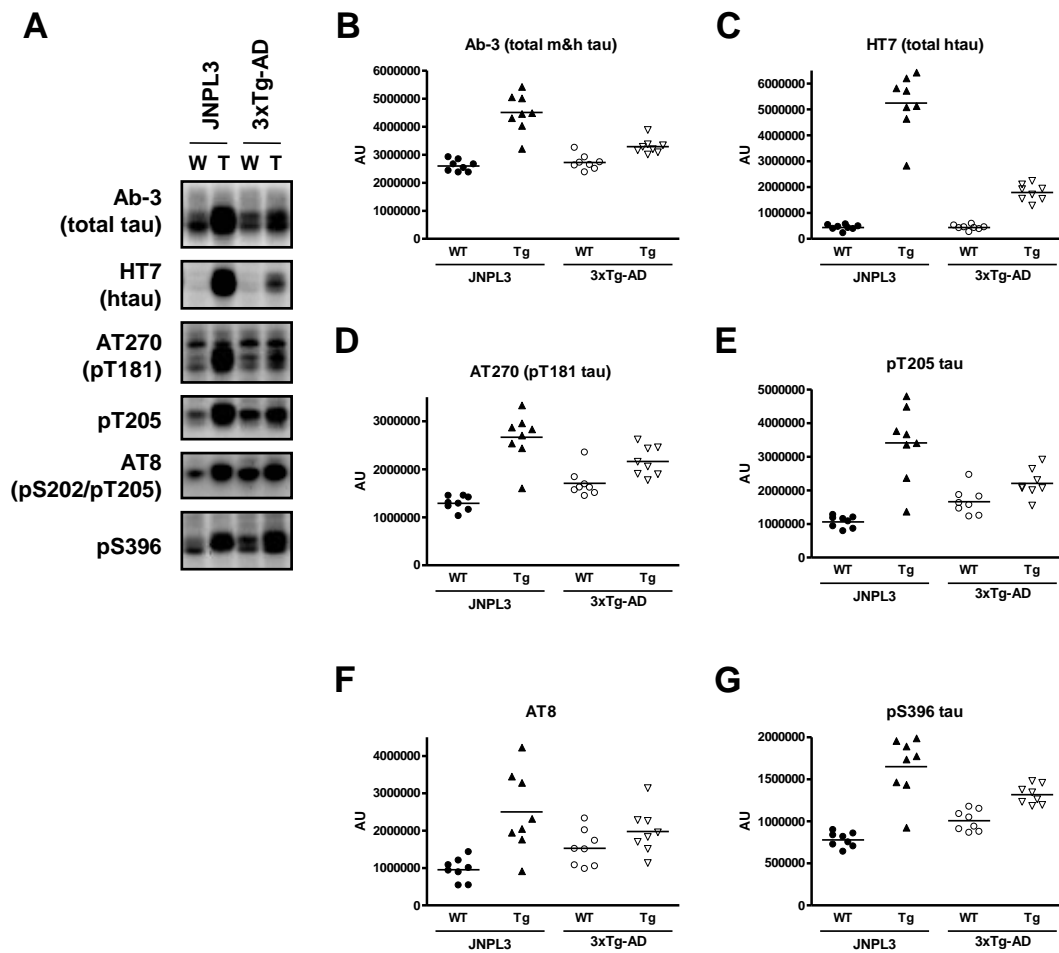
A**B**

Figure17. Behavioral improvement in a novel object recognition test after MMBO administration in 3xTg-AD mice. MMBO (1 and 3 mg/kg, b.i.d) or vehicle was administered for 24 days, 30 minutes prior to the acquisition phase. Exploration of a novel object was evaluated during retention phase, 5 hours after acquisition. Novel object recognition performance is shown as exploration frequency (A) or novel object preference ratio (B). Data were expressed as mean \pm SEM and analyzed statistically as follows: Student's *t*-test (novel object vs. familiar object or WT vs. Tg, * $p \leq 0.05$, ** $p \leq 0.01$, *** $p \leq 0.001$) and one-tailed Williams' test (vs. vehicle, # $p \leq 0.025$), $n = 10$.



Supplementary Figure 8. Amounts of tau in JNPL3 and 3xTg-AD mice. Total mouse and human tau, total human tau, and tau phosphorylated at T205, S396, T181, and S202/T205 were determined by immunoblot analysis (A). Quantitative comparisons of JNPL3 and 3xTg-AD mice are shown respectively in B-G. Data are expressed as scatter plots, n = 7 or 8.



General Discussion

In this study, I tried to examine the relationship between tau and etiology in neurodegenerative disease such as AD by generating a novel Tg mouse model (part 1), and I also tested potential of tau-targeting drug, which has been originally discovered (part 2). Tau, a MT protein is a key molecule in neurodegenerative diseases because it is accumulated as NFTs in a diseased brain and mutations in tau gene is known to cause a familial type of neurodegenerative disease (Hutton et al., 1998; Poorkaj et al., 1998; Spillantini et al., 1998). Toxicity of tau is not completely understood yet, however, hyperphosphorylation or mutations of tau is known to reduce the binding to MT through conformation change (Grundke-Iqbal et al., 1986; Goedert et al., 1995; Dan and Hasegawa., 2011). Detachment of tau from MT could destabilize MT and impair axonal function. Increased soluble pool of tau with mutation or hyperphosphorylation is prone to aggregate and it would damage neurons. Namely, mislocalization of tau might a key event in neurodegenerative diseases.

In part 1 of this study, a novel mutant tau Tg mouse TPR50 was generated and evaluated biochemically and behaviorally to analyze tau-induced neurotoxicity. TPR50 mouse dramatically displayed neurodegenerative disease-like phenotype such as age-dependent tau aggregation, motor dysfunction, and shortened life expectancy (Figures 1, 4 and 5, and Supplementary Figure 2). Additionally, impaired axonal transport as well as behavioral abnormality was clearly observed at early onset (Figures 6 and 9). Interestingly, as axonal dysfunction precedes obvious appearance of NFT-like pathology, increase in soluble and phosphorylated tau may perturb axonal function. Actually, it has been recently emphasized that soluble tau like oligomers plays an important role in neuronal dysfunction (Wittmann et al., 2001; SantaCruz et al., 2005; Cárdenas-Aguayo Mdel et al., 2014). Although molecular mechanism underlying axonal

impairment in TPR50 is still unknown, overexpressed mutant tau may interfere in function of endogenous tau and induce axonal dysfunction. In this study, MT hyperdynamism and increase in MT-related proteins were observed (Figures 7 and 8). Those observations might reflect imbalanced turnover of MT due to overload of mutant tau. Based on this result, it is hypothesized that targeting mislocalization of tau could be a promising therapeutic approach via reducing intracellular soluble tau oligomers and rescuing axonal function.

As one of candidate therapeutic approaches, inhibition of tau phosphorylation was focused in part 2. I discovered a novel inhibitor for GSK-3, a major kinase for tau, by efforts in the high-throughput screening and chemistry modification, and named MMBO. MMBO displays good selectivity for GSK-3, bioavailability, and brain permeability (Saitoh et al., 2009b and Table 2). Moreover, MMBO significantly showed therapeutic potential with reduction of tau phosphorylation and behavioral amelioration in AD mouse model (Figures 13 and 16), suggesting inhibition of tau phosphorylation would be a valid therapeutic strategy for AD as per the hypothesis. Regarding tau accumulation, MMBO did not change HT7-positive (total tau) pathology significantly (Figure 14). Therefore, observed behavioral amelioration could be dependent on reduction of soluble phosphorylated tau rather than effect of tau aggregate. This is consistent with my observation in TPR50 in part 1. In this study, I did not examine effect of MMBO on axonal transport or MT function. However, recent paper indicated that overexpression of tau with phosphomimetic mutations impaired axonal transport of mitochondria greater than WT tau (Shahpasand et al., 2012), suggesting that inhibition of tau phosphorylation might improve axonal function. Interestingly, pathological tau can enhance KLC phosphorylation by GSK-3 through activation of PP1

and following GSK-3 activation. KLC phosphorylation dissociates kinesin from cargo vesicles and impairs kinesin-dependent axonal transport (LaPointe et al., 2009; Kanaan et al., 2011). Namely, GSK-3 activation and consequent tau phosphorylation could lead to a vicious circle on axonal function. While, regarding dynein-dependent retrograde transport, tau accumulation might also impair it by affecting dynein/dynactin complex as reported by the recent study using flies (Butzlaff et al., 2015). Future study using MMBO will clarify relationship between tau phosphorylation and axonal function and the mechanism of action in its therapeutic effect.

In conclusion, improvement of axonal dysfunction due to abnormal tau is a novel therapeutic concept in neurodegenerative diseases such as AD, and inhibition of tau phosphorylation is a promising approach based on the concept.

Acknowledgements

I am most grateful to Professors Osamu Numata and Kazuto Nakata, and Associate Professors Kentaro Nakano and Kazuichi Sakamoto, University of Tsukuba, for their continuous guidance and valuable discussions through my doctoral program.

I thank Dr. Frank M. LaFerla for providing 3xTg-AD mice, KineMed, Inc. and Mr. Yoji Ueda for measurement of MT dynamics, Drs. Keisuke Hirai, Shinichi Kondou, Ken-ichi Noguchi, Tadatoshi Hashimoto, Hideaki Nagaya, and Takeo Wada for their encouragement, and Mr. Ryota Maeda, Ms. Yumiko Uno, Mr. Shunya Suzuki, Dr. Hideki Matsui, Mr. Masashi Yamaguchi, Dr. Keiji Yamamoto, Dr. Tomohiro Kawamoto, and Dr. Hideki Takahashi for helpful discussions.

References

Allen B, Ingram E, Takao M., Smith MJ, Jakes R, Virdee K, Yoshida H, Holzer M., Craxton M, Emson PC, Atzori C, Migheli A, Crowther RA, Ghetti B, Spillantini MG, Goedert M. (2002). Abundant tau filaments and nonapoptotic neurodegeneration in transgenic mice expressing human P301S tau protein. *J. Neurosci.* **22**, 9340–9351.

Alzheimer's Disease International: World Alzheimer Report 2015, Available in <http://www.alz.co.uk/research/world-report-2015>

alz.org: alzheimer's association a (<http://www.alz.org/dementia/types-of-dementia.asp>)

alz.org: alzheimer's association b (<http://www.alz.org/jp/dementia-alzheimers-japan.asp>)

Asami-Odaka A, Ishibashi Y, Kikuchi T, Kitada C, Suzuki N. (1995). Long amyloid beta-protein secreted from wild-type human neuroblastoma IMR-32 cells. *Biochemistry* **34**, 10272-10278.

Aplin AE, Gibb GM, Jacobsen JS, Gallo JM, Anderton BH. (1996). In vitro phosphorylation of the cytoplasmic domain of the amyloid precursor protein by glycogen synthase kinase-3beta. *J Neurochem.* **67**, 699-707.

Barten DM, Fanara P, Andorfer C, Hoque N, Wong PY, Husted KH, Cadelina GW, Decarr LB, Yang L, Liu V, Fessler C, Protassio J, Riff T, Turner H, Janus CG, Sankaranarayanan S, Polson C, Meredith JE, Gray G, Hanna A, Olson RE, Kim SH, Vite GD, Lee FY, Albright CF. (2012). Hyperdynamic microtubules, cognitive deficits, and pathology are improved in tau transgenic mice with low doses of the microtubule-stabilizing agent BMS-241027. *J. Neurosci.* **32**, 7137–7145.

Belarbi K, Schindowski K, Burnouf S, Caillierez R, Grosjean ME, Demeyer D, Hamdane, M, Sergeant N, Blum D, Buée L. (2009). Early Tau pathology involving the septo-hippocampal pathway in a Tau transgenic model: relevance to Alzheimer's disease. *Curr Alzheimer Res.* **6**, 152–157.

Belarbi K, Burnouf S, Fernandez-Gomez FJ, Desmercières J, Troquier L, Brouillette J, Tsambou L, Grosjean ME, Caillierez R, Demeyer D, Hamdane M., Schindowski K, Blum D, Buée L. (2011). Loss of medial septum cholinergic neurons in THY-Tau22 mouse model: what links with tau pathology? *Curr Alzheimer Res.* **8**, 633–638.

Bellucci A, Luccarini I, Scali C, Prosperi C, Giovannini MG, Pepeu G, Casamenti F. (2006). Cholinergic dysfunction, neuronal damage and axonal loss in TgCRND8 mice. *Neurobiol Dis.* **23**, 260–272.

Billings LM, Oddo S, Green KN, McGaugh JL. and LaFerla FM. (2005). Intraneuronal Abeta causes the onset of early Alzheimer's disease-related cognitive deficits in transgenic mice. *Neuron* **45**, 675-688.

Black MM, Baas PW, Humphries S. (1989). Dynamics of alpha-tubulin deacetylation in intact neurons. *J. Neurosci.* **9**, 358–368.

Brunden KR, Zhang B, Carroll J, Yao Y, Potuzak JS, Hogan AM, Iba M, James MJ, Xie S, Ballatore C, Smith AB. 3rd, Lee VM, Trojanowski JQ. (2010). Epothilone D improves microtubule density, axonal integrity, and cognition in a transgenic mouse model of tauopathy. *J. Neurosci.* **30**, 13861–13866.

Bugiani O, Murrell JR, Giaccone G, Hasegawa M, Ghigo S, Tabaton M, Morbin M, Primavera A, Carella F, Solaro C, Grisoli M, Savoiaro M, Spillantini MG, Tagliavini F, Goedert M, Ghetti B. (1999). Frontotemporal dementia and corticobasal degeneration in a family with a P301S mutation in Tau. *J Neuropathol Exp Neurol.* **58**, 667–677

Bullock BP. and Habener JF. (1998). Phosphorylation of the cAMP response element binding protein CREB by cAMP-dependent protein kinase A and glycogen synthase kinase-3 alters DNA-binding affinity, conformation, and increases net charge. *Biochemistry* **37**, 3795-3809.

- Butzlaff M, Hannan SB, Karsten P, Lenz S, Ng J, Voßfeldt H, Prüßing K, Pflanz R, Schulz JB, Rasse T, Voigt A.** (2015). Impaired retrograde transport by the Dynein/Dynactin complex contributes to Tau-induced toxicity. *Hum Mol Genet.* **24**, 3623-3637
- Caccamo A, Oddo S, Tran LX, and LaFerla FM.** (2007). Lithium reduces tau phosphorylation but not A beta or working memory deficits in a transgenic model with both plaques and tangles. *Am. J. Pathol.* **170**, 1669-1675.
- Cárdenas-Aguayo Mdel C, Gómez-Virgilio L, DeRosa S, Meraz-Ríos MA** (2014). The role of tau oligomers in the onset of Alzheimer's disease neuropathology. *ACS Chem Neurosci.* **5**, 1178-91.
- Chalecka-Franaszek E. and Chuang DM.** (1999). Lithium activates the serine/threonine kinase Akt-1 and suppresses glutamate-induced inhibition of Akt-1 activity in neurons. *Proc. Natl. Acad. Sci. USA* **96**, 8745-8750.
- Clinton LK, Billings LM, Green KN, Caccamo A, Ngo J, Oddo S, McGaugh JL, and LaFerla FM.** (2007). Age-dependent sexual dimorphism in cognition and stress response in the 3xTg-AD mice. *Neurobiol. Dis.* **28**, 76-82.
- Cole AR, Knebel A, Morrice NA, Robertson LA, Irving AJ, Connolly CN, and Sutherland C.** (2004). GSK-3 phosphorylation of the Alzheimer epitope within collapsin response mediator proteins regulates axon elongation in primary neurons. *J Biol Chem.* **279**, 50176-50180.
- Cruz JC, and Tsai LH.** (2004). A Jekyll and Hyde kinase: roles for Cdk5 in brain development and disease. *Curr. Opin. Neurobiol.* **14**, 390-394.
- Dan A, and Hasegawa M.** (2011). Molecular biology of FTDP-17 (frontotemporal dementia and parkinsonism linked to chromosome 17). *Nihon Rinsho.* **69** Suppl 10(Pt 2),

379-83.

Davies SP, Reddy H, Caivano Mm and Cohen P. (2000) Specificity and mechanism of action of some commonly used protein kinase inhibitors. *Biochem. J.* **351**, 95-105.

Dixit R, Ross JL, Goldman YE, and Holzbaur EL. (2008). Differential regulation of dynein and kinesin motor proteins by tau. *Science.* **319**, 1086–1089.

Drechsel DN, Hyman AA, Cobb MH, and Kirschner MW. (1992). Modulation of the dynamic instability of tubulin assembly by the microtubule-associated protein tau. *Mol Biol Cell.* **3**, 1141–1154.

Eckermann K, Mocanu MM, Khlistunova I, Biernat J, Nissen A, Hofmann A, Schönig K, Bujard H, Haemisch A, Mandelkow E, Zhou L, Rune G, and Mandelkow EM. (2007). The beta-propensity of Tau determines aggregation and synaptic loss in inducible mouse models of tauopathy. *J. Biol. Chem.* **282**, 31755–31765.

Engel T, Hernandez F, Avila J, and Lucas JJ. (2006). Full reversal of Alzheimer's disease-like phenotype in a mouse model with conditional overexpression of glycogen synthase kinase-3. *J. Neurosci.* **26**, 5083-5090.

Fanara P, Banerjee J, Hueck RV, Harper MR, Awada M, Turner H, Husted KH, Brandt R, and Hellerstein MK. (2007). Stabilization of hyperdynamic microtubules is neuroprotective in amyotrophic lateral sclerosis. *J. Biol. Chem.* **282**, 23465–23472.

Fanara P, Husted KH, Selle K, Wong PY, Banerjee J, Brandt R, and Hellerstein MK. (2010). Changes in microtubule turnover accompany synaptic plasticity and memory formation in response to contextual fear conditioning in mice. *Neuroscience.* **168**, 167–178.

Fanara P, Wong PY, Husted KH, Liu S, Liu VM, Kohlstaedt LA, Riiff T, Protasio JC, Boban D, Killion S, Killian M, Epling L, Sinclair E, Peterson J, Price RW, Cabin DE,

Nussbaum RL, Brühmann J, Brandt R, Christine CW, Aminoff MJ, and Hellerstein MK. (2012). Cerebrospinal fluid-based kinetic biomarkers of axonal transport in monitoring neurodegeneration. *J Clin. Invest.* **122**, 3159–3169.

Flunkert S, Hierzer M, Löffler T, Rabl R, Neddens J, Duller S, Schofield EL, Ward MA, Posch M, Jungwirth H, Windisch M, and Hutter-Paier B. (2013). Elevated Levels of Soluble Total and Hyperphosphorylated Tau Result in Early Behavioral Deficits and Distinct Changes in Brain Pathology in a New Tau Transgenic Mouse *Model*. *Neurodegener. Dis.* **11**, 194–205

Friedhoff P, von Bergen M, Mandelkow EM, and Mandelkow E. (2000). Structure of tau protein and assembly into paired helical filaments. *Biochim. Biophys. Acta.* **1502**, 122-132.

Gilman S, Koller M, Black RS, Jenkins L, Griffith SG, Fox NC, Eisner L, Kirby L, Rovira MB, Forette F, and Orgogozo JM; AN1792(QS-21)-201 Study Team. (2005). Clinical effects of Abeta immunization (AN1792) in patients with AD in an interrupted trial. *Neurology* **64**, 1553-1562.

Gimenez-Llort L, Blazquez G, Canete T, Johansson B, Oddo S, Tobena A, LaFerla FM, and Fernandez-Teruel A. (2007). Modeling behavioral and neuronal symptoms of Alzheimer's disease in mice: a role for intraneuronal amyloid. *Neurosci. Biobehav. Rev.* **31**, 125-147.

Goedert M, Wischikm CM, Crowther RA, Walker JE, and Klug A. (1988). Cloning and sequencing of the cDNA encoding a core protein of the paired helical filament of Alzheimer disease: identification as the microtubule-associated protein tau. *Proc Natl Acad Sci U S A.* **85**, 4051–4055.

Goedert M, Spillantini MG, Jakes R, Crowther RA, Vanmechelen E, Probst A, Götz J,

- Bürki K, and Cohen P.** (1995). Molecular dissection of the paired helical filament. *Neurobiol Aging*. **16**, 325–334.
- Goedert M, Jakes R, and Crowther RA.** (1999). Effects of frontotemporal dementia FTDP-17 mutations on heparin-induced assembly of tau filaments. *FEBS. Lett.* **450**, 306–311.
- Golde TE, Schneider LS, and Koo EH.** (2011). Anti-A β therapeutics in Alzheimer's disease: the need for a paradigm shift. *Neuron*. 2011 **69** , 203-213.
- Götz J, and Ittner LM.** (2008). Animal models of Alzheimer's disease and frontotemporal dementia. *Nat Rev Neurosci.* **9**, 532–544.
- Grundke-Iqbal I, Iqbal K, Tung YC, Quinlan M, Wisniewski HM, and Binder LI.** (1986). Abnormal phosphorylation of the microtubule-associated protein tau in Alzheimer cytoskeletal pathology. *Proc. Natl. Acad. Sci. USA* **83**, 4913-4917.
- Hampel H, Ewers M, Bürger K, Annas P, Mörtberg A, Bogstedt A, Frölich L, Schröder J, Schönknecht P, Riepe MW, Kraft I, Gasser T, Leyhe T, Möller HJ, Kurz A, and Basun H.** (2009). Lithium trial in Alzheimer's disease: a randomized, single-blind, placebo-controlled, multicenter 10-week study. *J Clin Psychiatry.* **70**, 922-31.
- Hansen TO, Rehfeld JF, and Nielsen FC.** (2004). GSK-3 β reduces cAMP-induced cholecystokinin gene expression by inhibiting CREB binding. *Neuroreport* **15**, 841-845.
- Henthorn KS, Roux MS, Herrera C, and Goldstein LS.** (2011). A role for kinesin heavy chain in controlling vesicle transport into dendrites in *Drosophila*. *Mol Biol Cell.* **22**, 4038–4046.
- Hernández F, Borrell J, Guaza C, Avila J, and Lucas JJ.** (2002). Spatial learning deficit in transgenic mice that conditionally over-express GSK-3 β in the brain but do not form tau filaments. *J Neurochem.* **83**, 1529-1533.

Hooper C, Markevich V, Plattner F, Killick R, Schofield E, Engel T, Hernandez F, Anderton B, Rosenblum K, Bliss T, Cooke SF, Avila J, Lucas JJ, Giese KP, Stephenson J, and Lovestone S. (2007) Glycogen synthase kinase-3 inhibition is integral to long-term potentiation. *Eur J Neurosci.* **25**, 81-86.

Hurd DD, and Saxton WM. (1996). Kinesin mutations cause motor neuron disease phenotypes by disrupting fast axonal transport in *Drosophila*. *Genetics.* **144**, 1075–1085.

Hutton M, Lendon CL, Rizzu P, Baker M, Froelich S, Houlden H, Pickering-Brown S, Chakraverty S, Isaacs A, Grover A, Hackett J, Adamson J, Lincoln S, Dickson D, Davies P, Petersen RC, Stevens M, de Graaff E, Wauters E, van Baren J, Hillebrand M, Joosse M, Kwon JM, Nowotny P, Che LK, Norton J, Morris JC, Reed LA, Trojanowski J, Basun H, Lannfelt L, Neystat M, Fahn S, Dark F, Tannenberg T, Dodd PR, Hayward N, Kwok JB, Schofield PR, Andreadis A, Snowden J, Craufurd D, Neary D, Owen F, Oostra BA, Hardy J, Goate A, van Swieten J, Mann D, Lynch T, and Heutink P. (1998). Association of missense and 5'-splice-site mutations in tau with the inherited dementia FTDP-17. *Nature* **393**, 702–705.

Iritani S, Niizato K, and Emson PC. (2001). Relationship of calbindin D28K-immunoreactive cells and neuropathological changes in the hippocampal formation of Alzheimer's disease. *Neuropathology.* **21**, 162–167.

Ishihara T, Hong M, Zhang B, Nakagawa Y, Lee MK, Trojanowski JQ, and Lee VM. (1999). Age-dependent emergence and progression of a tauopathy in transgenic mice overexpressing the shortest human tau isoform. *Neuron* **3**, 751–762.

Ishihara T, Zhang B, Higuchi M, Yoshiyama Y, Trojanowski JQ, and Lee VM. (2001). Age-dependent induction of congophilic neurofibrillary tau inclusions in tau transgenic

mice. *Am. J. Pathol.* **158**, 555–562.

Ishizawa T, Sahara N, Ishiguro K, Kersh J, McGowan E, Lewis J, Hutton M, Dickson DW, and Yen SH. (2003). Co-localization of glycogen synthase kinase-3 with neurofibrillary tangles and granulovacuolar degeneration in transgenic mice. *Am. J. Pathol.* **163**, 1057-1067.

Ittner LM, Fath T, Ke YD, Bi M, van Eersel J, Li KM, Gunning P, and Götz J. (2008). Parkinsonism and impaired axonal transport in a mouse model of frontotemporal dementia. *Proc. Natl. Acad. Sci. USA.* **105**, 15997–16002.

Kanaan NM, Morfini GA, LaPointe NE, Pigino GF, Patterson KR, Song Y, Andreadis A, Fu Y, Brady ST, and Binder LI. (2011). Pathogenic forms of tau inhibit kinesin-dependent axonal transport through a mechanism involving activation of axonal phosphotransferases. *J. Neurosci.* **31**, 9858–9868.

Kidd M. (1963). Paired helical filaments in electron microscopy of Alzheimer's disease. *Nature* **197**, 192–193.

Kidd M. (1964). Alzheimer's disease: An electron microscopy study. *Brain* **87**, 307–320.

Klein PS, and Melton DA. (1996) A molecular mechanism for the effect of lithium on development. *Proc. Natl. Acad. Sci. USA* **93**, 8455-8459.

LaPointe NE, Morfini G, Pigino G, Gaisina IN, Kozikowski AP, Binder LI, Brady ST. (2009). The amino terminus of tau inhibits kinesin-dependent axonal transport: implications for filament toxicity. *J. Neurosci. Res.* **87**, 440–451.

Le Corre S, Klafki HW, Plesnila N, Hübinger G, Obermeier A, Sahagún H, Monse B, Seneci P, Lewis J, Eriksen J, Zehr C, Yue M, McGowan E, Dickson DW, Hutton M, and Roder HM. (2006) An inhibitor of tau hyperphosphorylation prevents severe motor impairments in tau transgenic mice. *Proc. Natl. Acad. Sci. USA* **103**, 9673-9678.

- Lee G, Cowan N, and Kirschner M. (1998). The primary structure and heterogeneity of tau protein from mouse brain. *Science*. **239**, 285–288.
- Lee VM, Goedert M, and Trojanowski JQ. (2001). Neurodegenerative tauopathies. *Annu Rev Neurosci*. **24**, 1121–1159.
- Lewis J, McGowan E, Rockwood J, Melrose H, Nacharaju P, Van Slegtenhorst M, Gwinn-Hardy K, Paul Murphy M, Baker M, Yu X, Duff K, Hardy J, Corral A, Lin WL, Yen SH, Dickson DW, Davies P, and Hutton M. (2000). Neurofibrillary tangles, amyotrophy and progressive motor disturbance in mice expressing mutant (P301L) tau protein. *Nat. Genet*. **25**, 402-405.
- Liu F, Iqbal K, Grundke-Iqbal I, and Gong CX. (2002). Involvement of aberrant glycosylation in phosphorylation of tau by cdk5 and GSK-3beta. *FEBS Lett*. **530**, 209-214.
- Lossos A, Reches A, Gal A, Newman JP, Soffer D, Gomori JM, Boher M, Ekstein D, Biran I, Meiner Z, Abramsky O, and Rosenmann H. (2003). Frontotemporal dementia and parkinsonism with the P301S tau gene mutation in a Jewish family. *J. Neurol*. **250**, 733–740.
- Lovestone S, Hartley CL, Pearce J, and Anderton BH. (1996). Phosphorylation of tau by glycogen synthase kinase-3 beta in intact mammalian cells: the effects on the organization and stability of microtubules. *Neuroscience* **73**, 1145-1157.
- Lucas JJ, Hernandez F, Gomez-Ramos P, Moran MA, Hen R, and Avila J. (2001). Decreased nuclear beta-catenin, tau hyperphosphorylation and neurodegeneration in GSK-3beta conditional transgenic mice. *EMBO J*. **20**, 27-39.
- Murray ME, Lowe VJ, Graff-Radford NR, Liesinger AM, Cannon A, Przybelski SA, Rawal B, Parisi JE, Petersen RC, Kantarci K, Ross OA, Duara R, Knopman DS, Jack

CR Jr, and Dickson DW. (2015). Clinicopathologic and 11C-Pittsburgh compound B implications of Thal amyloid phase across the Alzheimer's disease spectrum. *Brain*. **138** (Pt 5), 1370-81.

Noble W, Olm V, Takata K, Casey E, Mary O, Meyerson J, Gaynor K, LaFrancois J, Wang L, Kondo T, Davies P, Burns M, Veeranna, Nixon R, Dickson D, Matsuoka Y, Ahljanian M, Lau LF, and Duff K. (2003). Cdk5 is a key factor in tau aggregation and tangle formation in vivo. *Neuron* **38**, 555-565.

Noble W, Planel E, Zehr C, Olm V, Meyerson J, Suleman F, Gaynor K, Wang L, LaFrancois J, Feinstein B, Burns M, Krishnamurthy P, Wen Y, Bhat R, Lewis J, Dickson D, and Duff K. (2005). Inhibition of glycogen synthase kinase-3 by lithium correlates with reduced tauopathy and degeneration in vivo. *Proc. Natl. Acad. Sci. USA*. **102**, 6990-6995.

Oddo S, Caccamo A, Shepherd JD, Murphy MP, Golde TE, Kaye R, Metherate R, Mattson MP, Akbari Y, and LaFerla FM. (2003). Triple-transgenic model of Alzheimer's disease with plaques and tangles: intracellular Abeta and synaptic dysfunction. *Neuron* **39**, 409-421.

Oddo S, Vasilevko V, Caccamo A, Kitazawa M, Cribbs DH, and LaFerla FM. (2006). Reduction of soluble Abeta and tau, but not soluble Abeta alone, ameliorates cognitive decline in transgenic mice with plaques and tangles. *J. Biol. Chem.* **281**, 39413-39423.

Onishi T, Iwashita H, Uno Y, Kunitomo J, Saitoh M, Kimura E, Fujita H, Uchiyama N, Kori M, and Takizawa M. (2011). A novel glycogen synthase kinase-3 inhibitor 2-methyl-5-(3-{4-[(S)-methylsulfinyl]phenyl}-1-benzofuran-5-yl)-1,3,4-oxadiazole decreases tau phosphorylation and ameliorates cognitive deficits in a transgenic model of Alzheimer's disease. *J. Neurochem.* **119**, 1330-1340.

Palop JJ, Chin J, Roberson ED, Wang J, Thwin MT, Bien-Ly N, Yoo J, Ho KO, Yu GQ, Kreitzer A, Finkbeiner S, Noebels JL, and Mucke L. (2007). Aberrant excitatory neuronal activity and compensatory remodeling of inhibitory hippocampal circuits in mouse models of Alzheimer's disease. *Neuron* **55**, 697-711.

Pei JJ, Tanaka T, Tung YC, Braak E, Iqbal K, and Grundke-Iqbal I. (1997). Distribution, levels, and activity of glycogen synthase kinase-3 in the Alzheimer disease brain. *J. Neuropathol. Exp. Neurol.* **56**, 70-78.

Pei JJ, Braak E, Braak H, Grundke-Iqbal I, Iqbal K, Winblad B, and Cowburn RF. (1999). Distribution of active glycogen synthase kinase 3beta (GSK-3beta) in brains staged for Alzheimer disease neurofibrillary changes. *J. Neuropathol. Exp. Neurol.* **58**, 1010-1019.

Peineau S, Taghibiglou C, Bradley C, Wong TP, Liu L, Lu J, Lo E, Wu D, Saule E, Bouschet T, Matthews P, Isaac JT, Bortolotto ZA, Wang YT, and Collingridge GL. (2007). LTP inhibits LTD in the hippocampus via regulation of GSK3beta. *Neuron* **53**, 703-717.

Pérez M, Hernández F, Lim F, Díaz-Nido J, and Avila J. (2003). Chronic lithium treatment decreases mutant tau protein aggregation in a transgenic mouse model. *J. Alzheimers. Dis.* **5**, 301-308.

Phiel CJ, and Klein PS. (2001). Molecular targets of lithium action. *Annu. Rev. Pharmacol. Toxicol.* **41**, 789-813.

Phiel CJ, Wilson CA, Lee VM, and Klein PS. (2003). GSK-3alpha regulates production of Alzheimer's disease amyloid-beta peptides. *Nature* **423**, 435-439.

Poorkaj P, Bird TD, Wijsman E, Nemens E, Garruto RM, Anderson L, Andreadis A, Wiederholt WC, Raskind M, and Schellenberg GD. (1998). Tau is a candidate gene for chromosome 17 frontotemporal dementia. *Ann. Neurol.* **43**, 815-825.

Riascos D, de Leon D, Baker-Nigh A, Nicholas A, Yukhananov R, Bu J, Wu CK, and Geula C. (2011). Age-related loss of calcium buffering and selective neuronal vulnerability in Alzheimer's disease. *Acta. Neuropathol.* **122**, 565–576.

Roberson ED, Scearce-Levie K, Palop JJ, Yan F, Cheng IH, Wu T, Gerstein H, Yu GQ, and Mucke L. (2007). Reducing endogenous tau ameliorates amyloid beta-induced deficits in an Alzheimer's disease mouse model. *Science* **316**, 750-754.

Rockenstein E, Torrance M, Adame A, Mante M, Bar-on P, Rose JB, Crews L, and Masliah E. (2007). Neuroprotective effects of regulators of the glycogen synthase kinase-3beta signaling pathway in a transgenic model of Alzheimer's disease are associated with reduced amyloid precursor protein phosphorylation. *J. Neurosci.* **27**, 1981-1991.

Ryder J, Su Y, Liu F, Li B, Zhou Y, and Ni B. (2003). Divergent roles of GSK3 and CDK5 in APP processing. *Biochem Biophys Res Commun* **312**, 922-929.

Sahara N, Vega IE, Ishizawa T, Lewis J, McGowan E, Hutton M, Dickson D, and Yen SH. (2004). Phosphorylated p38MAPK specific antibodies cross-react with sarkosyl-insoluble hyperphosphorylated tau proteins. *J. Neurochem.* **90**, 829–838.

Saitoh M, Kunitomo J, Kimura E, Hayase Y, Kobayashi H, Uchiyama N, Kawamoto T, Tanaka T, Mol CD, Dougan DR, Textor GS, Snell GP, and Itoh F. (2009a). Design, synthesis and structure-activity relationships of 1,3,4-oxadiazole derivatives as novel inhibitors of glycogen synthase kinase-3beta. *Bioorg Med Chem.* **17**, 2017-29.

Saitoh M, Kunitomo J, Kimura E, Iwashita H, Uno Y, Onishi T, Uchiyama N, Kawamoto T, Tanaka T, Mol CD, Dougan DR, Textor GP, Snell GP, Takizawa M, Itoh F, and Kori M. (2009b) 2-{3-[4-(Alkylsulfinyl)phenyl]-1-benzofuran-5-yl}-5-methyl-1,3,4-oxadiazole derivatives as novel inhibitors of glycogen synthase kinase-3beta with good brain

permeability. *J Med Chem.* **52**, 6270-86.

Santacruz K, Lewis J, Spires T, Paulson J, Kotilinek L, Ingelsson M, Guimaraes A, DeTure M, Ramsden M, McGowan E, Forster C, Yue M, Orne J, Janus C, Mariash A, Kuskowski M, Hyman B, Hutton M, and Ashe KH. (2005). Tau suppression in a neurodegenerative mouse model improves memory function. *Science* **309**, 476-481.

Sato S, Tatebayashi Y, Akagi T, Chui DH, Murayama M, Miyasaka T, Planel E, Tanemura K, Sun X, Hashikawa T, Yoshioka K, Ishiguro K, and Takashima A. (2002). Aberrant tau phosphorylation by glycogen synthase kinase-3beta and JNK3 induces oligomeric tau fibrils in COS-7 cells. *J. Biol. Chem.* **277**, 42060-42065.

Shahpasand K, Uemura I, Saito T, Asano T, Hata K, Shibata K, Toyoshima Y, Hasegawa M, Hisanaga S. (2012). Regulation of mitochondrial transport and inter-microtubule spacing by tau phosphorylation at the sites hyperphosphorylated in Alzheimer's disease. *J Neurosci.* **32**, 2430-2441.

Sperber BR, Leight S, Goedert M, and Lee VM. (1995). Glycogen synthase kinase-3 beta phosphorylates tau protein at multiple sites in intact cells. *Neurosci. Lett.* **197**, 149-153.

Spillantini MG, Murrell JR, Goedert M, Farlow MR, Klug A, and Ghetti B. (1998). Mutation in the tau gene in familial multiple system tauopathy with presenile dementia. *Proc. Natl. Acad. Sci. U. S. A.* **95**, 7737-7741.

Stokin GB, Lillo C, Falzone TL, Brusch RG, Rockenstein E, Mount SL, Raman R, Davies P, Masliah E, Williams DS, and Goldstein LS. (2005). Axonopathy and transport deficits early in the pathogenesis of Alzheimer's disease. *Science* **307**, 1282-1288.

Su Y, Ryder J, Li B, Wu X, Fox N, Solenberg P, Brune K, Paul S, Zhou Y, Liu F, and Ni B. (2004). Lithium, a common drug for bipolar disorder treatment, regulates amyloid-beta precursor protein processing. *Biochemistry* **43**, 6899-6908.

Takeuchi H, Iba M, Inoue H, Higuchi M, Takao K, Tsukita K, Karatsu Y, Iwamoto Y, Miyakawa T, Suhara T, Trojanowski JQ, Lee VM, and Takahashi R. (2011). P301S mutant human tau transgenic mice manifest early symptoms of human tauopathies with dementia and altered sensorimotor gating. *PLoS. One.* **6**, e21050.

Taniguchi S, Suzuki N, Masuda M, Hisanaga S, Iwatsubo T, Goedert M, and Hasegawa M. (2005). Inhibition of heparin-induced tau filament formation by phenothiazines, polyphenols, and porphyrins. *J. Biol. Chem.* **280**, 7614–7623.

Uno Y, Iwashita H, Tsukamoto T, Uchiyama N, Kawamoto T, Kori M, and Nakanishi A. (2009). Efficacy of a novel, orally active GSK-3 inhibitor 6-Methyl-N-[3-[[3-(1-methylethoxy)propyl]carbamoyl]-1H-pyrazol-4-yl]pyridine-3-carboxamide in tau transgenic mice. *Brain Res.* **3**, 1296:148-63.

Wagner U, Utton M, Gallo JM, and Miller CC. (1996). Cellular phosphorylation of tau by GSK-3 beta influences tau binding to microtubules and microtubule organization. *J. Cell Sci.* **109**, 1537-1543.

Wang JZ, Grundke-Iqbal I, and Iqbal K. (2007). Kinases and phosphatases and tau sites involved in Alzheimer neurofibrillary degeneration. *Eur. J. Neurosci.* **25**, 59-68.

Wang Y, Zhang JX, Du XX, Zhao L, Tian Q, Zhu LQ, Wang SH, and Wang JZ. (2008). Temporal correlation of the memory deficit with Alzheimer-like lesions induced by activation of glycogen synthase kinase-3. *J Neurochem.* **106**, 2364-2374.

Werber E, Klein C, Grünfeld J, and Rabey JM. (2003). Phenotypic presentation of frontotemporal dementia with Parkinsonism-chromosome 17 type P301S in a patient of Jewish-Algerian origin. *Mov. Disord.* **18**, 595–598.

Wisniewski HM, Narang HK, and Terry RD. (1976). Neurofibrillary tangles of paired helical filaments. *J Neurol Sci.* **27**, 173–181.

Wittmann CW, Wszolek MF, Shulman JM, Salvaterra PM, Lewis J, Hutton M, and Feany MB. (2001). Tauopathy in *Drosophila*: neurodegeneration without neurofibrillary tangles. *Science* **293**, 711-714.

Yasuda M, Yokoyama K, Nakayasu T, Nishimura Y, Matsui M, Yokoyama T, Miyoshi K, and Tanaka C. (2000). A Japanese patient with frontotemporal dementia and parkinsonism by a tau P301S mutation. *Neurology* **55**, 1224-1227.

Yoshimura T, Kawano Y, Arimura N, Kawabata S, Kikuchi A, and Kaibuchi K. (2005). GSK-3beta regulates phosphorylation of CRMP-2 and neuronal polarity. *Cell* **120**, 137-149.

Yoshiyama Y, Higuchi M, Zhang B, Huang SM, Iwata N, Saido TC, Maeda J, Suhara T, Trojanowski JQ, and Lee VM. (2007). Synapse loss and microglial activation precede tangles in a P301S tauopathy mouse model. *Neuron*. **53**, 337-351.

Zhang B, Higuchi M, Yoshiyama Y, Ishihara T, Forman MS, Martinez D, Joyce S, Trojanowski JQ, and Lee VM. (2004). Retarded axonal transport of R406W mutant tau in transgenic mice with a neurodegenerative tauopathy. *J. Neurosci.* **24**, 4657-4667.

Zhang B, Maiti A, Shively S, Lakhani F, McDonald-Jones G, Bruce J, Lee EB, Xie SX, Joyce S, Li C, Toleikis PM, Lee VM, and Trojanowski JQ. (2005). Microtubule-binding drugs offset tau sequestration by stabilizing microtubules and reversing fast axonal transport deficits in a tauopathy model. *Proc. Natl. Acad. Sci. USA.* **102**, 227-231.

Zhang B, Carroll J, Trojanowski JQ, Yao Y, Iba M, Potuzak JS, Hogan AM, Xie SX, Ballatore C, Smith AB. 3rd, Lee VM, and Brunden KR. (2012). The microtubule-stabilizing agent, epothilone d, reduces axonal dysfunction, neurotoxicity, cognitive deficits, and Alzheimer-like pathology in an interventional study with aged tau transgenic mice. *J. Neurosci.* **32**, 3601-3611.

Zhang F, Phiel CJ, Spece L, Gurvich N, and Klein PS. (2003). Inhibitory phosphorylation of glycogen synthase kinase-3 (GSK-3) in response to lithium. Evidence for autoregulation of GSK-3. *J. Biol. Chem.* **278**, 33067-33077.

Zhou FQ, Zhou J, Dedhar S, Wu YH, and Snider WD. (2004). NGF-induced axon growth is mediated by localized inactivation of GSK-3beta and functions of the microtubule plus end binding protein APC. *Neuron* **42**, 897-912.